Sediment Transport and Floods In A Changing Climate

A Numerical Study of the Relationship Between Rainfall Intensity and Sediment Transport in Rivers with a Morphodynamic Model

Lars Fredrik Kirkebø Lund

M.Sc Thesis in Applied and Computational Mathematics

Department of Mathematics
University of Bergen

June 2020

Acknowledgements

I would like to thank my supervisor Gerard Dam for his invaluable guidance, feedback and patience while working on this thesis, and for sharing his knowledge and expertise. Thank you for introducing me to the world of floods, morphodynamics and computer modelling.

Many thanks to Jarle Berntsen for his constructive feedback, writing-advice and meetings.

Finally, I want to thank my friends and family for their support over the years. The moral support from home, and the study sessions and lunch-breaks at the university, have been valued highly.

Lars Fredrik, June 2020

Abstract

Rainfall intensity and river flood magnitudes in Norway are expected to increase in the near future due to climate change. This thesis investigates the morphological impacts this increase in rainfall intensity will have on pluvial river flood events. The 2-D numerical morphologic model FINEL2D is applied to 3 scenarios, with 5-hour rainfall courses of different intensities. To explore the differences between hydrologic and morphologic models, parallel simulations with the morphologic module turned off are carried out for comparison. Special attention is given to the effect that differences in slope in a river have on sediment transport. Reliability of morphologic models, and their applications in river flood maps, are discussed.

The simulation results imply an exponential relationship between rainfall intensity and sediment transport in rivers. A 50% increase in rainfall intensity results in a doubling of transported sediment. The differences between a morphologic and hydrologic simulation amounts to significant variations in flood-levels and flow extension based on the terrain and river layout. Differences in slope is identified as a driving factor of morphological changes. Sediment is eroded from steep segments of a river and causes sedimentation in flatter areas. The model strives towards an equilibrium in flow conditions, and thus flattens out differences in slopes. Morphological models are able to

accurately hindcast morphological changes over time. It is argued that the behavior of morphological models to find an equilibrium, makes them in large part able to predict morphological changes in a flood event. Even with the strong non-linear behavior and added uncertainties, a morphologic model has several benefits over a hydrologic model, making them potentially valuable in flood maps. The importance of morphological models may become even more relevant with a future increase in rainfall intensity caused by climate change, which results in larger morphological changes in a flood event.

Contents

Chapter 1

Introduction, Research Questions and Outline

Floods have the potential to cause large damage to human life and property through the movement of water and sediment. Projections of future changes in climate by Klimaservicesenteret (Hansen-Bauer, 2015) and the Norwegian Water Resources and Energy Directorate (NVE) (Lawrence, 2016), indicate a significant increase in rainfall intensity, leading up to the year 2100. This may increase the magnitude of floods in western and northern Norway caused by short, high intensity, rainfall, by up to 60% (Hansen-Bauer, 2015; Lawrence, 2016). To mitigate the damages caused by these floods, it is important to develop an understanding of which factors causes floods, and the potential impacts they may have. Taking measures based on this understanding is tied to the notions of flood risk, flood maps and flood management (Plate, 2002).

Historically, flood mapping and risk management was conducted by collecting data and studying previous flooding events in a specific river or watercourse (Brázdil et al., 2006). Since these accounts may contain errors in dating,

interpretation, or may have originated from questionable sources, the accuracy is unreliable, and generally boiled down to a problem of recurrence. The modern development of hydrodynamic equations and models, as well as the introduction of computers, have changed the way flood maps are constructed. The ability to simulate different scenarios with a hydrologic model enables us to more effectively make risk-assessments in terms of safety and cost (Tsakiris, 2014). There are many different models used in flood mappings, where each one has its advantages and drawbacks. For practical results with low computational cost in an area with a simple geometric layout, a 1-D hydrologic scheme may be applied, while for areas with more complex terrain demands more comprehensive modelling with a 2-D, or possibly 3-D, scheme (Tsakiris, 2014).

It is debated whether a model which only considers hydrologic conditions is sufficient, or if the incorporation of models with morphodynamic modules in flood maps are necessary (Guan et al., 2015, 2016; Wong et al., 2014; Slater et al., 2015). The non-linear models used, in conjunction with uncertainties in boundary conditions and insufficient data, poses problems of accuracy and reliability (Beven, 2001) when using hydrologic models, which might be amplified by the incorporation of a non-linear morphodynamic module in the modelling (Wong et al., 2014; Haff, 1996). However, with the future increase in rainfall and flood magnitudes (Midttømme, 2011), the amount of sediment moved in floods is likely to increase exponentially (Mohamadi & Kavian, 2015), making the debate of whether to use a morphologic model in flood maps more relevant.

Research Questions and Outline

In this thesis, the following research questions are examined:

What impact does an increase in rainfall intensity, caused by climate change, have on sediment transport in a river flood event?

What effects do differences in slope have on sediment transport?

What are the differences between a hydrologic and a morphologic model?

Are morphologic models reliable, and should they be used in flood maps?

This will be achieved by using a 2-D morphological model on 3 scenarios, with varying rainfall intensities. To investigate and discuss the effects of incorporating a morphodynamic module in flood simulations, parallel hydrological simulations will be run for comparison.

The outline of the thesis is as follows:

Chapter 2 - An overview of important river characteristics, floods and morphology are introduced. Examples of floods in Norway, with large amounts of sediment being transported, are presented for. The examples are later used to put the simulation results into a broader realistic context. A basic outline of how flood maps are created in Norway is described briefly discussed.

Chapter 3 - The model used in the simulations, the governing equations

and boundary conditions used are described. This includes both the hydrological module, based on the depth-integrated shallow water equations, and the sediment transport module.

Chapter 4 - The model setups used in the simulations are described, and the computational grids, boundary values, bathymetry and rainfall courses are presented. Results from the simulations are, in order, presented and described.

Chapter 5 - The results are put into context and discussed from the perspective of existing litterature. Morphologic models and their reliability are discussed.

Chapter 6 - The findings are summarized, and the concluding remarks are given.

Chapter 2

Sediment Transport, Floods and Flood maps

2.1 Sediment Transport

Descriptions of elementary river characteristics and sediment transport are based mostly on the works of Allen (1997), Easterbrook (1996) and Rawlins (1995).

In areas where precipitation is not all evaporated, the excess water flows to the ocean or gathers in other locations based on the geometry of the terrain, e. g. lakes. This flow is mainly through rivers and streams, either from the precipitation going directly into the water course, or through indirect means, such as going into ground water first and by overland flow. Another important contributor to these flows in Norway is the melting of glaciers. However, the focus of this thesis is on flow caused by precipitation.

Rivers vary greatly in their characteristics, such as flow rate, length, width,

slopes, curvature and build-up of sediment. Over time, however, these characteristics change. Erosion on the banks of a river may lead to a higher capacity flow, sedimentation may lead to a narrowing of the channel, thus increasing velocity of the flow, or the erosion may make the bed deeper. Over long time scales (centuries/millennia), these changes may make rivers shift position and curvature entirely. In cases off extreme events in rivers with large quantities of available sediment, such as a flood event caused by intense precipitation, these changes may occur over the course of hours.

For rivers that do not flow directly over bedrock, the bed is comprised of sediment. This layer of sediment can range from a few centimeters above bedrock, to a scale of several meters. During a flood event, this sediment is available for further transport (Dewals et al., 2011). Long term morphology in the river is dependent on the build-up of this sediment. Finer sediments, such as silt and sand, are more easily picked up and transported downstream, while heavier particles such as gravel and rocks tend to bounce along the bottom only if the flow velocity is large enough.

This sediment transport can be placed in three different categories; wash load, suspended load, and bed load, where the last two are the most relevant in the study of morphodynamic changes in floods. The wash load is fine sediment that floats on the river surface. Suspended load is sediment that is carried in the water column due to the turbulent nature of the flow, where the settling velocity is approximately equal to the vertical velocity, due to drag and lift forces on the particles. If the settling velocity is higher than the vertical velocity, the sediment bounces along the bottom as bed load.

Whether an individual particle is transported as suspended load or as bed-load is dependent on particle size, weight, shape and on flow conditions. Because the forces acting on the sediment is dependent on flow conditions, an increase in flow velocity results in an increase in sediment transport. Empirical transport formulae describe the relationship between flow velocity and sediment transport with a power function between 3 to 5 (van Rijn, 1993), meaning an increase in flow velocity of 15-25% results in a two-fold increase in sediment transport. Sediment transport is therefore most prominent in flows with high velocity. For movement of a sediment particle initiate, the forces acting on the particle must exceed the critical shear stress. This happens when the friction and inertia forces on a particle exceeds the bed shear stress of the river. Bottom load is thus heavily dependent on the friction in the river bed.

The flood plain is the area in the vicinity of the banks in which the river overflows onto. The spreading of river water over this area causes the wash load and suspended load to deposit. Over time an equilibrium may arise, where the amount of sediment eroded from the banks and floodplains is balanced by the sediment carried on-land by flooding in the river Blom et al. (2017). These areas are especially suited for agriculture, due the constant addition of fertile soils from the river. Because of this, many farms are settled in these areas, making them particularly vulnerable to extreme floods.

The longitudinal profile is important for determining flow velocities, since steeper slopes leads to higher velocities, resulting in more sediment transport. This profile is represented by plotting the elevation above a base line, usually above sea level, to the distance of the river mouth. Most longitudi-

nal profiles are concave upward. This happens due to the reduction in flow velocity when the river runs into a body of still water such as a lake or the sea, and the suspended sediment and bedload is sequentially deposited in this area Sinha & Parker (1996). This area is called a river delta.

2.2 Floods in Norway

Floods in Norway are usually caused by rainfall, snow melting, or a combination of the two. Over the last decade, there have been an estimated 3 billion NOK in damages caused by floods in Norway, with yearly insurance claims on the scale of hundreds of millions of NOK (*Naturskader*, 2019). Settlements and infrastructure located in steep catchments are especially vulnerable, due to the high velocities and sediment masses involved (Midttømme, 2011).

Figure 2.1: Aftermath of the flood from Storelva in Utvik. The river diverted through the town and caused large amounts of sediment and debris to deposit. *Photo:Vågenes H. (2017)*

The flood in Storelva in Utvik, Sogn of Fjordane, on the 24th of July 2017, was the result of heavy rainfall (Figure 2.1). Typical for small rivers in Norway, data such as rainfall intensity, water levels and discharge rates are not available because of the lack of measurements. Sediment blockages in the main channel, in combination with the high discharge rates, caused the

flow to divert and create new channels through the town. Hydrologic and morphologic simulations of the event were later carried out by Dam (2017), with the model used in this thesis. The hydrologic simulation was unable to predict the formation of the new channels, while the morphologic simulation resembled reality much more closely. Particularly noticeable is the sedimentation and debris in the town, where the erosion and sedimentation caused by the flood is depicted in figure (Figure 2.2).

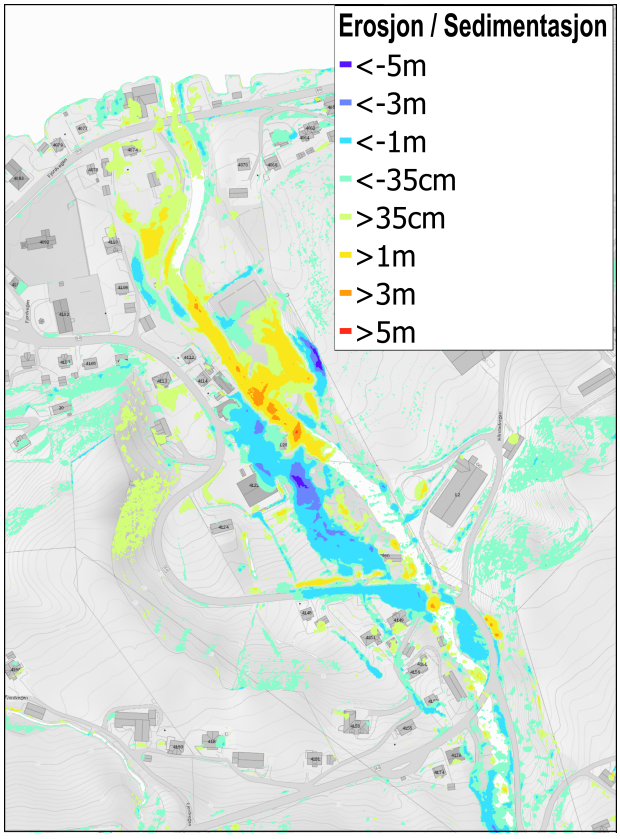

Figure 2.2: Erosion and sedimentation caused by the flood event in Utvik.

Figure 2.3: The flood in Flåm. There is considerable erosion on the banks of the river, endangering and destroying several houses. *Photo:Mikalsen (2014)*

In Flåm, on the 28th of October 2014, heavy rainfall and snow melting in the mountains caused Flåmselva to overflow it banks. Unlike the flood in Utvik, the flood did not divert and create new channels, but instead, heavy erosion of the banks occurred (Figure 2.3). The foundations beneath the houses located in the flood plains were eroded away, and whole buildings were carried downstream. The bridge (Figure 2.3) could not withstand the masses of water and sediment, and clogged up, before it eventually collapsed and was taken by the flood.

One of the most devastating flood events in recent Norwegian history is Vesleofsen, in June 1995. The flood was caused by a combination of large amounts of snow melting, and heavy rainfall. The flood event spanned several rivers and lakes in eastern Norway. In Tretten, the river Moksa experienced extremely high discharges, causing the river to divert course completely, flowing

Figure 2.4: The flood in Tretten. The river Moksa diverted through the town, causing erosion of house foundations and sedimentation in the town.*Photo:Eeg J. (1995)*

through the town center (Figure 2.4). Not only did the river divert through the town like in Utvik, but the foundations of the residences were also eroded away, similarly to the flood in Flåm, leading to several houses being carried away by the flood.

2.3 Flood maps in Norway

Since 2007, Norway has been under the European Union's flood directive. The Norwegian Water Resources and Energy Directorate (NVE) has, in accordance with this directive, developed guidelines for development and planning and development in risk prone areas along watercourses in Norway (Midttømme, 2011; Nie, 2012). These guidelines are developed in agreement with civil engineering regulations (TEK-regulations).

The severity of the flood is set by its recurrence. The recurrence is the average number of years between floods of a similar magnitude occur. The method of calculating this average can be based upon; observed water flow, the data of nearby stations where no such measures are available, historical regional flood frequency and precipitation/run-off models (Nie et al., 2012).

For floods, there are three safety classes: F1, F2 and F3, set by recurrence. A F1 flood has a 5% yearly likelihood of occurring, or once every 20 years. Areas with a F1 safety class allows for buildings with little human activity, or small economic or societal consequences in the case of a flood. The F2 safety class involves floods with a 0.5% yearly likelihood of occurring, or once every 200 years. In areas with a F2 safety class, building such a private residences, schools, industry and agriculture, are permitted. Even if economic damage to these areas can be large, critical societal functions remain intact. Buildings with critical societal functions are placed in the F3 safety class. A flood with F3 magnitude has a 0.1% yearly likelihood of occurring, or every 1000 years. Buildings with critical societal functions include old-age homes, hospitals, fire stations and police stations.

The TEK classifications are not as well-defined when an event involves large amounts of both sediment and water. These events can either fall into the flood categories, or in the categories for landslides: S1, S2, S3. These categories are defined in a similar way to the flood categories, however with recurrence intervals of 100, 1000, and 5000 years, for S1, S2, and S3, respectively. Slides triggered by water flow, or landslides ending up in a water course may fall under these categories.

Particularly dangerous are floods where landslides end up in a steep water course. Steep slopes allow for large amounts of sediment transport, with high velocity and force, making damages caused by these floods devastating. This sediment will deposit where the river flattens out or meets a choke point. The buildup of sediment pushes the water up and leads to overflowing and formation of new channels in the terrain (Figure 2.1). Human infrastructure and communities are often located around the flatter regions of a river and delta, making them particularly vulnerable to this overflowing and sedimentation (Midttømme, 2011)

Based on the guidelines provided by NVE, it is the municipalities' responsibility to create and maintain an accurate flood and landslide map of their local building and development areas rivers. To develop these flood maps, a hydrodynamic numerical model is frequently used, without a sediment transport module. Such models require geometrical data of the river and knowledge of constructions such as bridges, culverts and sluices along the watercourse. In addition, you need knowledge of e.g. the drainage capacity of the precipitation-areas and historical flood-record data.

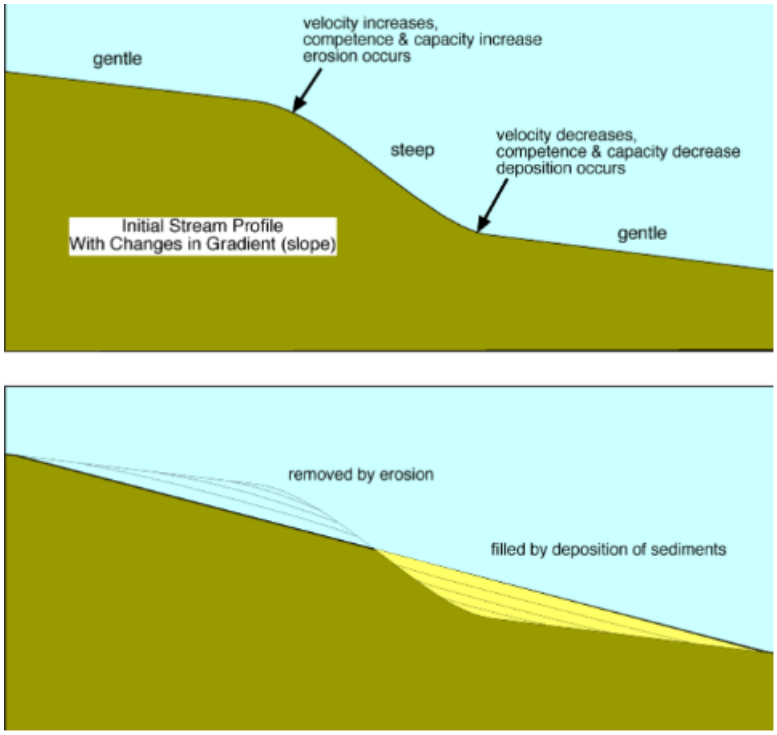

Figure 2.5: Representation of the slope effect on erosion and sedimentation. Sediment from the steep region, where the velocity is high, is eroded and deposited in the gentle region, where the velocity is decreased.

However, the use of hydrological models is a large simplification of reality, since it is obvious that changes in bed level occurs (Neuhold et al., 2009). Field evidence shows that extreme floods can cause significant changes in the river channel (Guan et al., 2015, 2016; Dam, 2017). Morphodynamics change the bed due to erosion and sedimentation, which causes direct changes in water-levels and inundation areas. This sedimentation and erosion are caused mostly by gradients in the flow velocity, where a river or stream is trying to reach an equilibrium (Figure 5.2). Sediment is eroded from river segments with steeper slopes, where the flow velocity is large, and

deposits when the slopes become gentler, where the flow velocity decreases.

Depending on the river characteristics and available sediment, flood maps can become obsolete over a period of hours, days or years. From papers such as Guan et al. (2015, 2016) one might assume that including morphology is crucial in all types of flood maps, and hydrology gives an insufficient overview of risks tied to floods. However, papers such as Wong et al. (2014) states that hydraulic models generally do not need to account for morphology in the flood itself, as these changes have a small impact compared to other uncertainties such as boundary conditions. The morphodynamic changes needs to happen over a series of events to have a large impact in certain types of river, such as a gravel-bed river with low amounts of available sediment (Guan et al., 2015).

Slater et al. (2015) found that changes in channel capacity, such as a narrow or widening of a river channel, may be a more important factor in flood hazard than changes in streamflow, e.g. higher flow velocity or volume flux. Although sudden changes in streamflow, such as from a dam breach, rainstorms or melting of glaciers, poses a greater flood hazard, effects of changes in channel capacity are more common. They also found that flow frequency and channel capacity changes flood hazard over time. This undermines the use of historical records in flood mapping, as those advised by NVE, by means of probability distribution functions based on the recurrence of floods in that river, since boundary conditions and flow changes over time. In other words, looking at past events does not necessarily contribute to future predictions of floods (Slater et al., 2015). This questions the applicability of classifying floods based on their occurrence from the NVE guidelines, where it is especially true for longer recurrences (F2, F3).

Morphodynamic changes are dependent on the sediment available for erosion and transport, and the importance of morphodynamics in flood maps must be determined on a case-by-case basis from the build-up of the bed and river hydrology. Wong et al. (2014); Guan et al. (2015, 2016) and Slater et al. (2015), all tried to better understand the influence of morphology during floods, with different views on the necessity of using morphological models in flood maps.

Chapter 3

The Model and Governing Equations

The model used for the simulations is FINEL2D (Dam et al., 2006, 2016; Dam, 2017), developed by Dutch company Svašek Hydraulics. The model uses the finite element method, dividing the computational domain into a finite number of 2-dimensional domains connected by nodal points. FINEL2D uses an unstructured triangular grid, allowing for more flexibility and accuracy in complex regions. These stationary domains acts as control volumes, where the governing equations are the shallow water equations (Vreugdenhil, 1994).

The shallow water equations are a system of hyperbolic partial differential equations describing fluid flow in areas where the vertical length scales are orders of magnitude smaller than the typical horizontal scales. The horizontal flow direction and the concept of balance of mass implies that vertical velocities are small in scale compared to horizontal velocity scales (Vreugdenhil, 1994). Thus, the conservation equations can be averaged over the depth

to represent a 3-dimensional domain with a 2-dimensional model. This simplification greatly reduces the computational cost of running the simulations. The shallow water equations are derived from the Navier-Stokes equations, which describes the motion of viscous fluids. The Navier-Stokes equations are derived from the physical equations for conservation of mass and balance of linear momentum (Kundu P., 2016).

In addition to a hydrodynamic module, the model also has a sediment transport module, allowing for estimations of morphological changes over time. Figure 3.1 depicts a time-step of the model when the morphodynamic module is activated. The flow conditions are first calculated, then the sediment transport is determined based on the flow conditions. The bed level of each computational cell is updated before the new flow conditions are calculated in the next time-step.

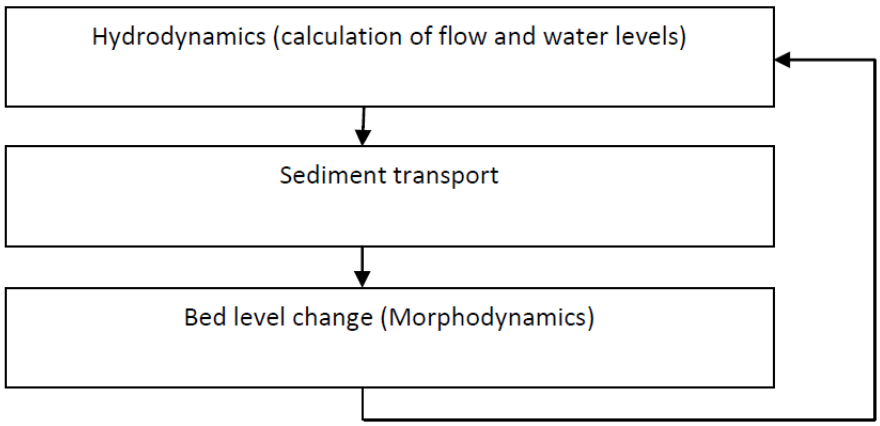

Figure 3.1: Representation of a time-step in the morphodynamic model.

3.1 Governing equations and boundary conditions

To derive the shallow water equations (Vreugdenhil, 1994), the Navier-Stokes equations for a Newtonian, non-compressible, fluid is considered:

$$\nabla \cdot \mathbf{v} = 0 \tag{3.1}$$

$$\frac{\partial}{\partial t}\rho\mathbf{v} + \nabla \cdot (\rho\mathbf{v}\mathbf{v}) = -\nabla p + \rho\mathbf{g} + \nabla \cdot \bar{\tau}, \tag{3.2}$$

where

$\mathbf{v} = \begin{pmatrix} u \\ v \\ w \end{pmatrix}$ is the fluid velocity vector [$\mathrm{m\,s^{-1}}$] in the x, y and z direction, respectively, where x and y are considered horizontal and z vertical

∇ is the del-operator

ρ is the fluid density [$\mathrm{kg\,m^{-3}}$]

$\mathbf{g}$ is the gravitational acceleration vector [$\mathrm{m\,s^{-2}}$]

p is the pressure [Pa]

$\bar{\tau}$ is the stress tensor [$\mathrm{N\,m^{-2}}$]

A typical water column is represented in Figure 3.2, where

$\zeta = \zeta(t, x, y)$ is the level [m] of the free surface relative to the geoid where $z = 0$

$b = b(t, x, y)$ is the bathymetry [m], where downward is the positive direction from the geoid

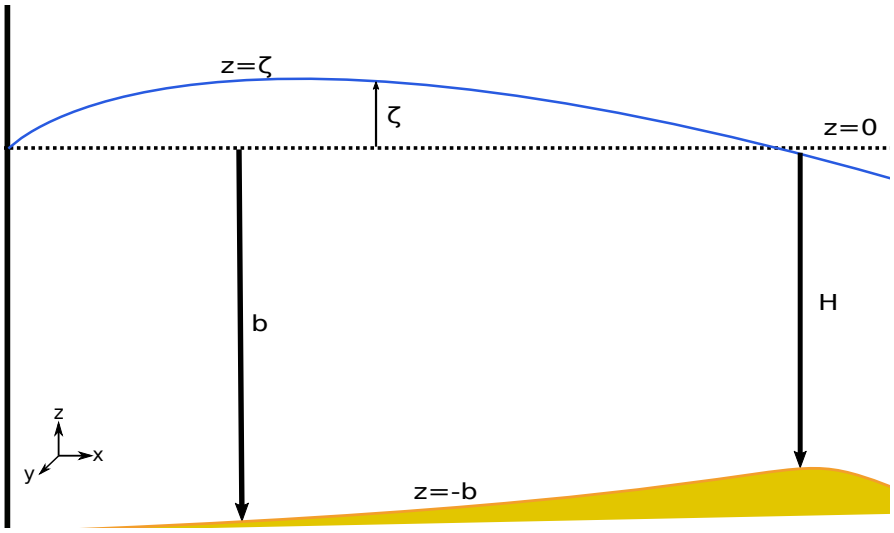

Figure 3.2: Representation of a water column

$H = H(t, x, y) = \zeta + b$ is the total depth [m] of the water column

At the bottom, where $z = -b$, the boundary conditions are as follows:

No slip:

$$u = v = 0 \tag{3.3}$$

No normal flow:

$$\frac{\partial b}{\partial t} + u\frac{\partial b}{\partial x} + v\frac{\partial b}{\partial y} + w = 0 \tag{3.4}$$

Bottom shear stress:

$$\tau_{bx} = \tau_{xx}\frac{\partial b}{\partial x} + \tau_{xy}\frac{\partial b}{\partial y} + \tau_{xz} \tag{3.5}$$

$$\tau_{by} = \tau_{yx}\frac{\partial b}{\partial x} + \tau_{yy}\frac{\partial b}{\partial y} + \tau_{yz}, \tag{3.6}$$

where τ_{bx} and τ_{by} are the specific bottom frictions, in the x and y direction, respectively.

At the free surface, where $z = \zeta$, the boundary conditions are:

Kinematic boundary condition:

$$\frac{\partial \zeta}{\partial t} + u\frac{\partial \zeta}{\partial x} + v\frac{\partial \zeta}{\partial y} - w = 0 \tag{3.7}$$

Dynamic boundary condition:

$$(p)_{z=\zeta} = 0 \tag{3.8}$$

Surface shear stress:

$$\tau_{sx} = -\tau_{xx}\frac{\partial \zeta}{\partial x} - \tau_{xy}\frac{\partial \zeta}{\partial y} + \tau_{xz} \tag{3.9}$$

$$\tau_{sy} = -\tau_{yx}\frac{\partial \zeta}{\partial x} - \tau_{yy}\frac{\partial \zeta}{\partial y} + \tau_{yz} \tag{3.10}$$

where τ_{sx} and τ_{sy} are the specific surface stresses (e.g. wind) in the x and y direction, respectively.

By the scaling argument (Vreugdenhil, 1994), all terms in the vertical momentum equation (3.2 are small, except for the pressure derivative and the gravity term. The z-momentum equation from 3.2 can then be reduced to

$$\frac{\partial p}{\partial z} = \rho g \tag{3.11}$$

which can be integrated over the water column, yielding

$$p = \rho g(\zeta - z). \tag{3.12}$$

This is known as the hydrostatic pressure distribution (Kundu P., 2016). 3.12 can be differentiated with respect to x and y, yielding the following expressions for the pressure terms:

$$\frac{\partial p}{\partial x} = \rho g\frac{\partial \zeta}{\partial x} \tag{3.13}$$

$$\frac{\partial p}{\partial y} = \rho g \frac{\partial \zeta}{\partial y} \tag{3.14}$$

3.2 The Shallow Water Equations

Depth-integrating the continuity equation (3.1) over the water column (Figure 3.2) from $z = -b$ to $z = \zeta$, using Leibniz's integral rule, yields:

$$0 = \int_{-b}^{\zeta} \nabla \cdot \mathbf{v} dz \tag{3.15}$$

$$= \int_{-b}^{\zeta} (\frac{\partial u}{\partial x} + \frac{\partial v}{\partial y}) dz + w\Big|_{z=\zeta} - w\Big|_{z=-b} \tag{3.16}$$

$$\begin{aligned} = \frac{\partial}{\partial x}\int_{-b}^{\zeta} u dz + \frac{\partial}{\partial y}\int_{-b}^{\zeta} v dz - \left(u\Big|_{z=\zeta}\frac{\partial \zeta}{\partial x} + u\Big|_{z=-b}\frac{\partial b}{\partial x}\right) \\ - \left(v\Big|_{z=\zeta}\frac{\partial \zeta}{\partial y} + v\Big|_{z=-b}\frac{\partial b}{\partial y}\right) + w\Big|_{z=\zeta} - w\Big|_{z=-b} \end{aligned} \tag{3.17}$$

Now, the boundary terms can be replaced, by using boundary conditions 3.4 and 3.7, with

$$\frac{\partial H}{\partial t} = \frac{\partial \zeta}{\partial t} + \frac{\partial b}{\partial t} \tag{3.18}$$

Finally, defining the depth-averaged velocities as

$$\bar{u} = \frac{1}{H}\int_{-b}^{\zeta} u dz \tag{3.19}$$

$$\bar{v} = \frac{1}{H}\int_{-b}^{\zeta} v dz \tag{3.20}$$

where

$\bar{u}$ is the depth-averaged velocity in the x-direction $[\mathrm{m\,s^{-1}}]$

$\bar{v}$ is the depth-averaged velocity in the y-direction $[\mathrm{m\,s^{-1}}]$

Combining these results gives the depth-integrated continuity equation:

$$\frac{\partial H}{\partial t} + \frac{\partial}{\partial x}(H\bar{u}) + \frac{\partial}{\partial y}(H\bar{v}) = 0 \tag{3.21}$$

Using 3.12 to collapse the z-momentum equation (3.2) makes it possible to substitute the pressure terms in the x- and y-momentum equations 3.2 with 3.13 and 3.14. Then, depth-integrating the left-hand side (LHS) of the x- and y-momentum equations 3.2, yields

$$\rho \int_{-b}^{\zeta} \left[\frac{\partial}{\partial t}u + \frac{\partial}{\partial x}u^2 + \frac{\partial}{\partial y}(uv) + \frac{\partial}{\partial z}(uw) \right] dz \qquad \text{(LHS x-momentum)}$$

$$= \rho \left(\frac{\partial}{\partial t}(H\bar{u}) + \frac{\partial}{\partial x}(H\bar{u}^2) + \frac{\partial}{\partial y}(H\bar{u}\bar{v}) + \Theta_{adv} \right)$$

$$\rho \int_{-b}^{\zeta} \left[\frac{\partial}{\partial t}v + \frac{\partial}{\partial x}(uv) + \frac{\partial}{\partial y}v^2 + \frac{\partial}{\partial z}(vw) \right] dz \qquad \text{(LHS y-momentum)}$$

$$= \rho \left(\frac{\partial}{\partial t}(H\bar{v}) + \frac{\partial}{\partial x}(H\bar{u}\bar{v}) + \frac{\partial}{\partial y}(H\bar{v}^2) + \Theta_{adv} \right),$$

where Θ_{adv} are the differential advection terms, accounting for the averaging over two functions.

On the right-hand side (RHS) of the momentum equations 3.2, depth-averaging yields

$$\int_{-b}^{\zeta} \left[\frac{\partial}{\partial t}v + \frac{\partial}{\partial x}(uv) + \frac{\partial}{\partial y}v^2 + \frac{\partial}{\partial z}(vw) \right] dz - \rho g H \frac{\partial \zeta}{\partial x} + \tau_{sx} - \tau_{bx} + \frac{\partial}{\partial x}\int_{-b}^{\zeta} \tau_{xx} + \frac{\partial}{\partial y}\int_{-b}^{\zeta} \tau_{xy}$$

(RHS x-momentum)

$$- \rho g H \frac{\partial \zeta}{\partial y} + \tau_{sy} - \tau_{by} + \frac{\partial}{\partial x}\int_{-b}^{\zeta} \tau_{xy} + \frac{\partial}{\partial y}\int_{-b}^{\zeta} \tau_{yy} \qquad \text{(RHS y-momentum)}$$

Using boundary conditions 3.6 and 3.10, rearranging, ignoring surface stresses and the advection terms and including equation 3.21 yields the hydrologic equations used in FINEL2D for the simulations in the thesis:

$$\boxed{\frac{\partial H}{\partial t} + \frac{\partial}{\partial x}(H\bar{u}) + \frac{\partial}{\partial y}(H\bar{v}) = 0} \tag{3.22}$$

$$\boxed{\frac{\partial}{\partial t}(H\bar{u}) + \frac{\partial}{\partial x}(H\bar{u}^2) + \frac{\partial}{\partial y}(H\bar{u}\bar{v}) + gH\frac{\partial \zeta}{\partial x} - \frac{1}{\rho}\tau_{x,b} = 0} \tag{3.23}$$

$$\boxed{\frac{\partial}{\partial t}(H\bar{v}) + \frac{\partial}{\partial x}(H\bar{u}\bar{v}) + \frac{\partial}{\partial y}(H\bar{v}^2) + gH\frac{\partial \zeta}{\partial x} - \frac{1}{\rho}\tau_{y,b} = 0} \tag{3.24}$$

where

$\bar{u}$ is the depth-averaged velocity in the x-direction [$\mathrm{m\,s^{-1}}$]

$\bar{v}$ is the depth-averaged velocity in the y-direction [$\mathrm{m\,s^{-1}}$]

$H = \zeta(t,x,y) + b(t,x,y)$ is the depth from the free surface to the bottom [m]

$b(t,x,y)$ is the depth from the free surface to the bottom [m]

$\zeta(t,x,y)$ is the bathymetry [m], where downward is the positive direction from the geoid

g is the gravitational acceleration [$\mathrm{m\,s^{-2}}$]

ρ is the density of water [$\mathrm{kg\,m^{-3}}$]

τ_b is the bottom shear stress [$\mathrm{N\,m^{-2}}$]

3.3 The Hydrodynamic module

The solving method in the hydrodynamic module is discontinuous Galerkin (Uzunca, 2016) with a cell-centered approach, where the flow variables are taken constant in each computational cell (Figure 3.3). The time-rate of change of mass and moment in each cell is calculated by the fluxes through the cell boundary, where the shallow water equations 3.22 , 3.23 and 3.24 are written as:

$$\frac{\partial \mathbf{U}}{\partial t} + \nabla \cdot \mathbf{F} = \mathbf{J}, \tag{3.25}$$

where

$$\mathbf{U} = \begin{pmatrix} \zeta \\ \bar{u}H \\ \bar{v}H \end{pmatrix}, \quad \mathbf{F} \begin{pmatrix} \bar{u}H & \bar{v}H \\ \bar{u}^2H + \frac{1}{2}g\zeta^2 & \bar{u}\bar{v}H \\ \bar{u}\bar{v}H & \bar{v}^2H + \frac{1}{2}g\zeta^2 \end{pmatrix}, \quad \mathbf{J} = \begin{pmatrix} 0 \\ \frac{1}{\rho}\tau_{x,tot} - gHi_{b,x} \\ \frac{1}{\rho}\tau_{y,tot} - gHi_{b,y} \end{pmatrix}$$

$\tau_{x,tot}$ and $\tau_{y,tot}$ are summations of the external stresses in x- and y-directions, $i_{b,x}$ and $i_{y,b}$ are the bed level gradients in x- and y-directions.

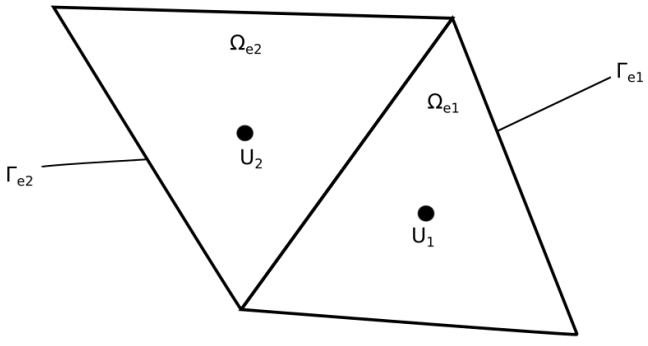

Figure 3.3: Representation of grid cells

3.25 can now be integrated over a triangular grid-cell, giving

$$\frac{d}{dt}\int_{\Omega_e} \mathbf{U} d\Omega + \int_{\Gamma_e} \mathbf{F}\mathbf{n} d\Gamma_e = \int_{\Omega_e} \mathbf{J} d\Omega \tag{3.26}$$

where Ω_e is a cell in the computational grid, Γ_e is its boundary, and $\mathbf{n}$ is the outward normal to Γ_e.

The problem is now reduced to determining the fluxes $\mathbf{F}$ along the boundaries of the cells. However, the flow variables are determined inside the cells, and not at the boundaries. Therefore the flux $\mathbf{F}$ is not unique, but must be found from the flow states of the cells adjacent to the boundaries $\Gamma_{e1} \cap \Gamma_{e2}$ (Figure 3.3). This means solving a local Riemann problem (Evans, 2010) along the boundary between the two cells, where the discontinuity is the boundary.

The Roe Approximate Riemann solver is used, based on the Godunov's scheme (Toro, 1999). This scheme ensures the conservation of mass and momentum. After the flux from the Riemann problem has been found, the solution $\mathbf{U}$ in each cell is updated using 3.25.

Forward Euler is used as the integrating scheme. On account of the explicit method, the time-step is chosen so that the Courant number is always less than 1 to ensure convergence, and controlled for automatically to optimize performance. The method is first order accurate in time and space.

3.4 The Sediment Transport module

Figure 3.4 depicts the sediment flux in the x-direction in a porous bed. The sediment balance over a slice of the bed can be expressed, ignoring for now suspended sediment, as

$$k\Delta x\Delta\eta = q_x(x)\Delta t - q_x(x+\Delta x)k\Delta t, \tag{3.27}$$

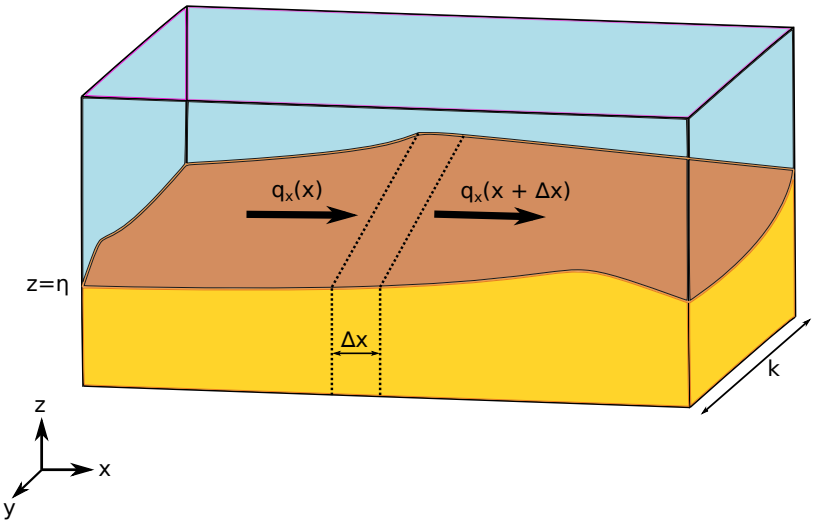

Figure 3.4: Representation of sediment flux

where

$\eta(t, x, y)$ is the bed elevation [m] (represents the same entity as b)

$\Delta\eta$ is the change in bed level [m]

k is the width of the bed slice [m]

Δx is the length of the bed slice [m]

Δt is a change in time [t]

$q_x(x)$ is sediment the in-flow over the bed slice [$\mathrm{m}^2\,\mathrm{s}^{-1}$]

$q_x(x + \Delta x)$ is the sediment out-flow over the bed slice [$\mathrm{m}^2\,\mathrm{s}^{-1}$]

This equation tells us that, the change between sediment in-flow and out-flow over the river bed slice of width k and length Δx, is accounted for in a change in bed-elevation, η. Now, dividing through by $k\Delta x\Delta t$ gives

$$\frac{\Delta\eta}{\Delta t} = -\left(\frac{q_x(x + \Delta x) - q_x(x)}{\Delta x}\right) \tag{3.28}$$

Taking the infinitesimal limit and rearranging gives

$$\frac{\partial \eta}{\partial t} + \frac{\partial q_x}{\partial x} = 0 \tag{3.29}$$

Extending this idea to include sediment flux in the y-direction, gives the bed level sediment balance equation used in the model;

$$\boxed{\frac{\partial \eta}{\partial t} + \frac{\partial q_x}{\partial x} + \frac{\partial q_y}{\partial y} = 0,} \tag{3.30}$$

where q_x and q_y are the sediment fluxes in the x- and y-direction, respectively. For the non-cohesive part of the sediment fluxes, the transport formula of Engelund F. (1967), 3.31, is used.

$$S = 0.05\mathbf{u}\frac{\sqrt{u^2+v^2}^4}{\sqrt{g}C^3\frac{(\rho_s-\rho)^2}{\rho^2}D_{50}} \tag{3.31}$$

where

S is the magnitude of the equilibrium sand transport $[\mathrm{m^2 s^{-1}}]$

$\mathbf{u} = \begin{pmatrix} u \\ v \end{pmatrix}$ is the fluid velocity vector in the x- and y-direction $[\mathrm{m\,s^{-1}}]$

u is the velocity in the x-direction $[\mathrm{m\,s^{-1}}]$

v is the velocity in the y-direction $[\mathrm{m\,s^{-1}}]$

g is the gravitational acceleration $[\mathrm{m\,s^{-2}}]$

$C = \frac{v_a}{\sqrt{RH_g}}$ is the Chèzy coefficient $[\mathrm{m^{1/2}\,s^{-1}}]$, where v_a is the average velocity, R is the hydraulic radius, H_g is the hydraulic gradient

ρ_s is the mass density of sand $[\mathrm{kg\,m^{-3}}]$

ρ is the mass density of water $[\mathrm{kg\,m^{-3}}]$

D_{50} is the grain size [m], meaning 50% of the sediment is finer than this value

The Engelund and Hansen formula is usually applied to rivers with fine sediment, since it does not account for a critical shear stress, meaning sediment is transported under any flow. This means it is not well-suited for rivers with coarse grain sizes. The modelling of the suspended sediment transport is done using the method of Galappatti and Vreugdenhil (Galappatti & Vreugdenhil, 1985); A dimensionless equilibrium concentration is calculated as

$$c_e = \frac{S}{H\sqrt{\bar{u}^2 + \bar{v}^2}}, \tag{3.32}$$

where

c_e is the equilibrium suspended load concentration

The depth-averaged suspended sediment concentration is then calculated from

$$H\left(\frac{\partial c}{\partial t} + u\frac{\partial c}{\partial x} + v\frac{\partial c}{\partial y}\right) = \frac{1}{T_c}\left[c_e(t) - c(t)\right], \tag{3.33}$$

where

H is the water depth [m]

c is the depth averaged suspended sediment concentration [-]

u and v are the horizontal velocities [$\mathrm{m\,s^{-1}}$]

c_e is the equilibrium suspended sediment concentration [-]

$T_c = \frac{\zeta}{v_s}$ is a characteristic time scale [s], where v_s is the settling velocity of the particles in water

Conservation of the bottom load, through 3.30, and suspended load, through 3.33, is thus accounted for. From 3.33, it is observed that erosion will occur if the sediment concentration is lower than the equilibrium concentration, and deposition if it is higher. The characteristic time scale reflects how quickly the concentration adjusts to an equilibrium. For shallow areas this timescale is usually small, and therefore it quickly returns to the equilibrium concentration.

Chapter 4

Simulations

4.1 Uniform gradient scenario

4.1.1 Computational grid, bathymetry and model settings

The uniform gradient scenario features a catchment area of $30\,\mathrm{km}^2$, where the computational grid and bathymetry are depicted in Figure 4.1 (a), and (b), respectively. This is a medium- to large-sized catchment area relative to other catchments in Norway. There is a straight river course going through the center of the grid, starting at y-coordinate 10000 and leading to the sea at y-coordinate 0, where the flow direction is downward. A part of the sea is included for sediment to deposit into. A constant water level of 0 is applied to the region below y-coordinate 0, meaning the water levels in the sea does not change.

The computational grid is produced by a grid-generating script. Boundary curves are drawn, then filled with triangles of desired cell sizes. Different

resolutions can be set for regions of interest, where smaller triangles yield more computational fidelity, at a higher cost. The script interpolates the areas of the triangles between different resolutions for a smoother grid. For this scenario, the resolution of the grid cells is set at $100\,\mathrm{m}^2$, with a finer resolution of $5\,\mathrm{m}^2$ applied in the river course. The grid has 46,325 elements, and the models' runtime is $\sim$45 minutes on a 2-core 2.30 GHz processor.

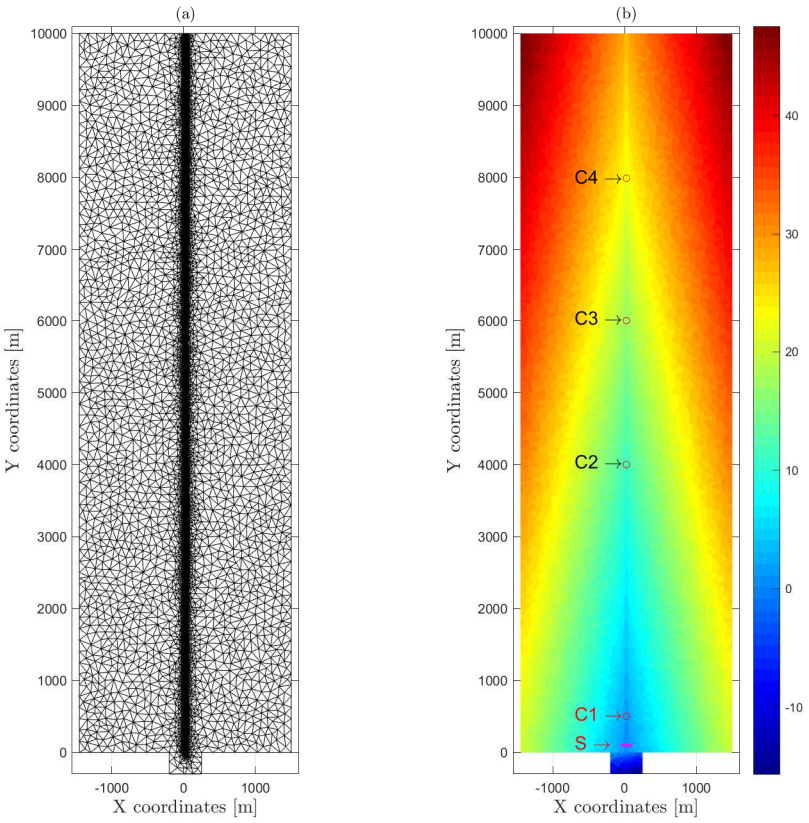

Figure 4.1: Computational grid for the uniform gradient scenario is depicted in (a), and bathymetry for the uniform gradient scenario, in meters above sea level, in (b). C indicates Control Stations, S indicates Sections.

A height-value is assigned to each triangle element in the computational grid to produce the bathymetry. The max height in the terrain is 48 m, down to a minimum of 0 m at the river outlet. A maximum depth of 15 m is applied in the sea, to allow for large amounts of sediment to deposit. Gradients in the surrounding terrain are 1.3% in the x-direction, and 0.28% in the y-direction, so that all runoff flow towards the river course. The river has a slope of 0.28%, meaning a gentle gradient, matching the surrounding terrain. There is a 1 m difference between the river course and the surrounding riverbanks. To avoid mass-erosion in certain cells, a maximum layer of 2 m is allowed to erode throughout the terrain.

In the simulations, a global (hydrological and morphological) roughness of 10 cm is used, based on the Nikuradse roughness equation (Nakayama, 2018). The roughness refers to the vertical variations in the surface, where surfaces such as asphalt roads and bare mountain have very low roughness (on a scale of millimeters or centimeters), while dense forest and vegetation has a higher roughness (on a scale of centimeters or decimeters). Roughness and flow variables, such as velocity and depth, are dependent on each other, making roughness variable under real world circumstances. A global roughness is used for simplicity.
The sediment is set as sand with D_{50}=1 cm, meaning that 50% of the sediment is finer than D_{50}. Mass density of sand is set at ρ_s=2650 kg m^{-3}.

Precipitation drives the model, where the runoff finds its way to the river. To investigate the morphologic effects of an increase in precipitation, the simulations are run with a base-line rainfall course (Run0) of 85 mm over 5 hours, then an incremental increase of 10%, up to 50% (Run1 through

Run/Hours	Hour 0-1	Hour 1-2	Hour 2-3	Hour 3-4	Hour 4-5	Morphology
Run0	10	15	30	20	10	On
Run1	11	16.5	33	22	11	On
Run2	12	18	36	24	12	On
Run3	13	19.5	39	26	13	On
Run4	14	21	42	28	14	On
Run5	15	22.5	45	30	15	On
Run0hyd	10	15	30	20	10	Off
Run5hyd	15	22.5	45	30	15	Off

Table 4.1: Represents rainfall courses used in the simulations, with units in mm.

Run5), is applied. The amount of rainfall in the simulations are represented in Table 4.1. In the simulations, all rainfall is available as runoff, meaning that the ground is taken as saturated from the start. Hydrologic simulations, Run0hyd and Run5hyd, were also carried out to investigate the difference between a morphologic and hydrologic simulation. The model allows for control stations and sections (Figure 4.1 (b)) which monitors flow variables and bottom development at certain points of interest over the simulation.

4.1.2 Results

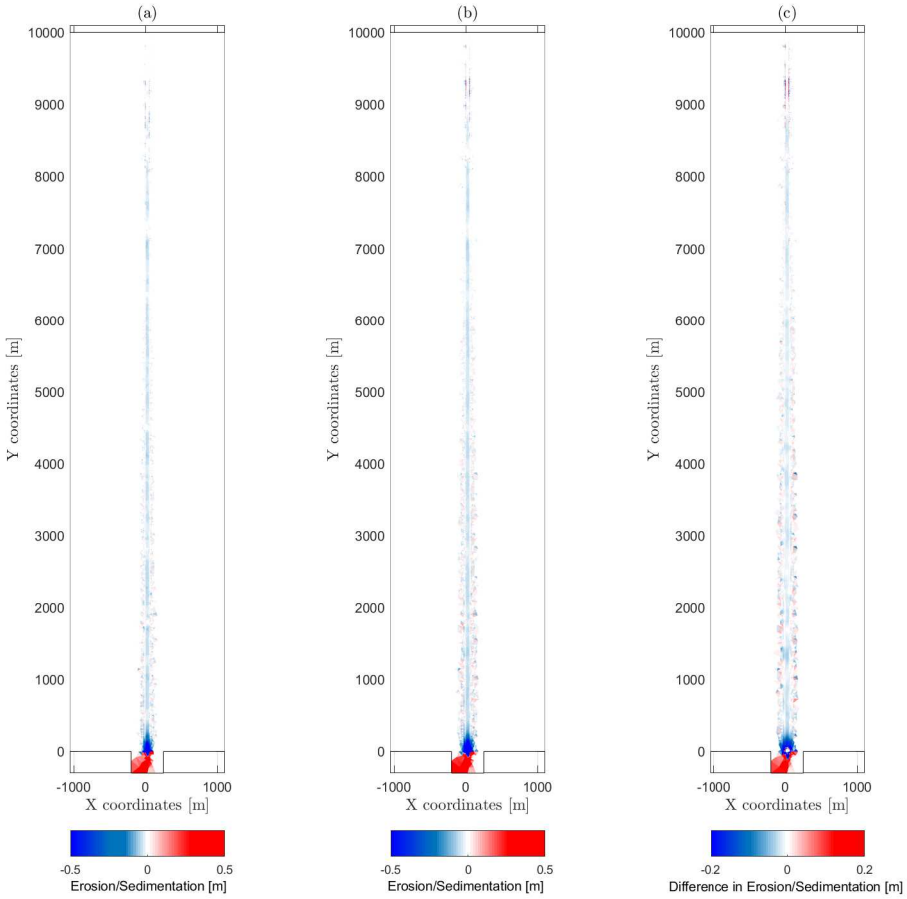

Figure 4.2: Erosion and sedimentation, in the Uniform Gradient Scenario, after 5 hours. The result from the baseline rainfall, Run0, is depicted in (a), and from a 50% increase in rainfall, Run5, in (b). The difference between (a) and (b) is shown in (c)

Figure 4.2 shows the morphologic changes after 5 hours of Run0 and Run5, as well as the difference between them. Throughout the river course there is erosion of the bed, amounting to a deepening of the river channel of several centimeters throughout, represented in Figure 4.3. Run0 and Run5 shows

similar trends in bed erosion, with Run5 being more pronounced. This erosion is due to the runoff carrying sediment further downstream, where most of it ultimately deposits in the sea.

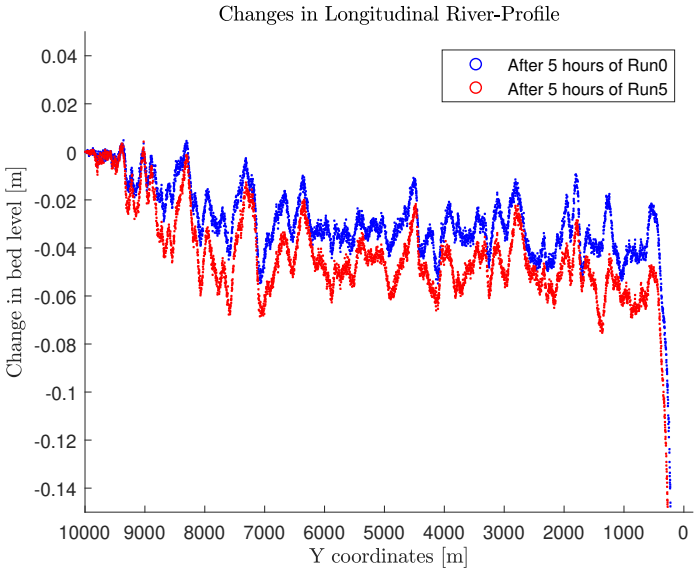

Figure 4.3: Changes in the longitudinal river profile after 5 hours of Run0 and Run5. Both show erosion throughout the river course, with Run5 being more pronounced.

Erosion occurs along the banks of the river (Figure 4.2), because the runoff does not enter the channel in the stream direction. The banks are eroded, and the sediment from the banks ends up in the river and is transported to the sea. Slight sedimentation occurs, most noticeable in Run5, along the banks of the river channel. This is from suspended load and gully wash from overflowing of the river channel which deposits in the floodplains. Most of the erosion along the banks occur further downstream, due to the catchment area being located along the river channel, instead of above it. Therefore the downstream parts of the river experience higher amounts of runoff, and

consequently erosion. The river mouth experiences more erosion, both of the bed and of the banks. The widening and deepening of the river channel allow for a higher water discharge, adjusting for the amount of runoff. A river delta is clearly forming, with sedimentation in the sea and widening of the river mouth (Figure 4.2). This formation is more pronounced in Run5. Most of the sedimentation occurring in the sea, observed in Figure 4.2, is on the left-hand side, even though the bathymetry is symmetrical around the river. This is caused by the low grid-resolution in this area, collecting most of the sediment in the large cells.

Changes in bed level occurring at Control Stations 1 through 4 over the 5-hour runs are shown in Figure 4.4. There is more erosion closer to the river mouth, at Station 1. The morphologic response for all runs and control stations start after the first hour, with an increase in precipitation showing a larger response. The slow response is due to the small amounts of rainfall during the first hour, the gentle slopes in the river and terrain, and the large catchment area. At Station 1 the difference in precipitation between run0 and run5 results in almost a threefold change in bed level, from 2 cm to 6 cm. Due to the Control Stations being situated in a single cell, qualitative trends are more important than individual quantitative changes of each run.

The rate of sediment discharge and cumulative discharge through Section S (Figure 4.1), near the river mouth, are represented in Figure 4.5. The discharge rate responds quickly to the hourly changes in precipitation, and all runs follow the same trends. This is due to the straight-river with uniform bed gradient used in the simulation, where most of the sediment is transported all the way to the sea before it deposits. Due to the negligible

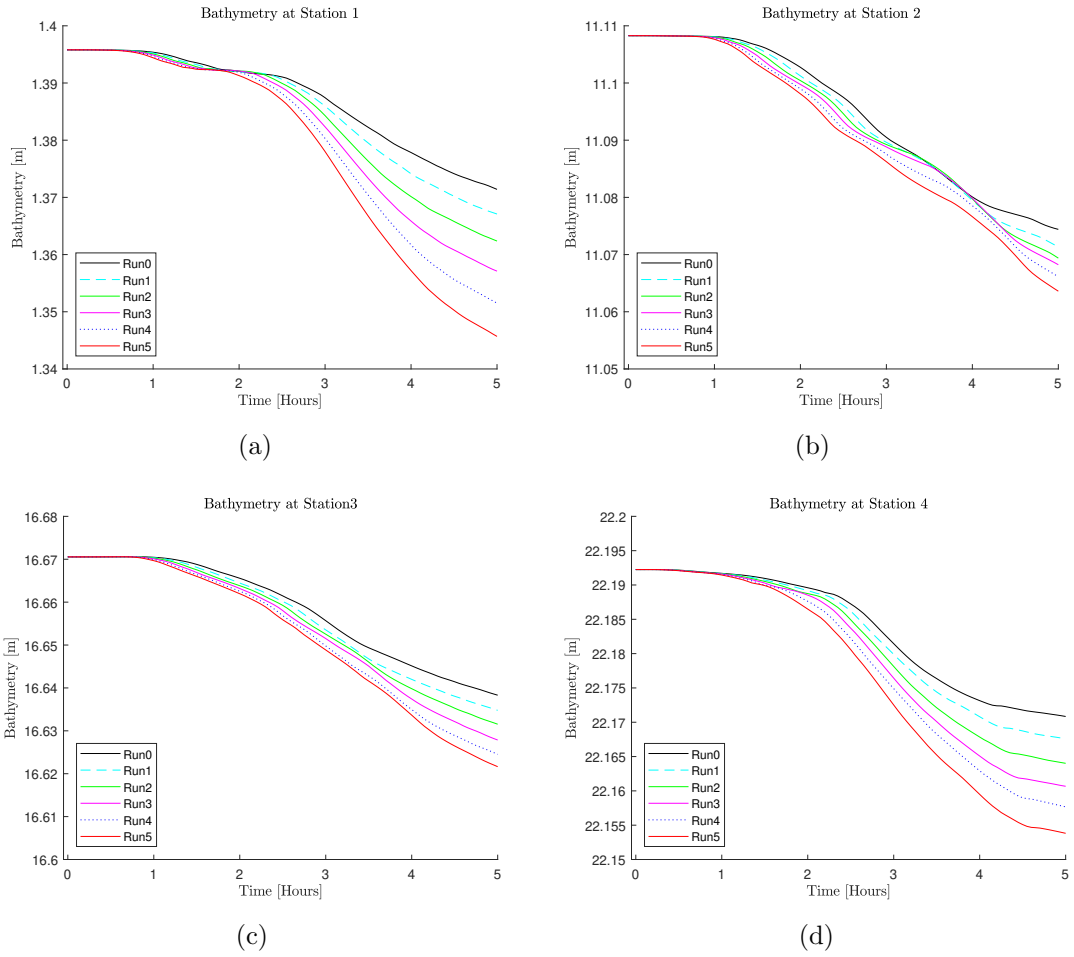

Figure 4.4: Bathymetry at Control Stations 1 through 4, over 5 hours. Shows Run0 through Run5. The Control Stations are indicated in Figure 4.1 (b)

sedimentation throughout the river channel, nearly all the sediment discharge is carried through Section S (Figure 4.1). Thus, from Figure 4.5 (b), it is concluded that a 50% increase in precipitation causes a doubling of sediment transported in this scenario. This means that, with an expected increase in rainfall (Hansen-Bauer, 2015), the effect of morphology on flood levels will become more important in the future.

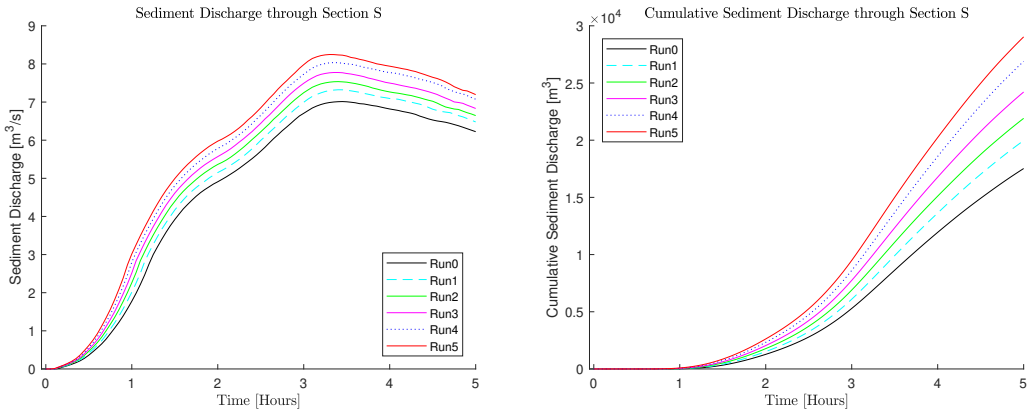

(a) (b)

Figure 4.5: Sediment discharge through Section 1 (a), and cumulative sediment discharge through Section S (b). Section S is indicated in Figure 4.1 (b).

The water depth at the end of Run0 and Run5, with and without morphology, is shown in Figure 4.6, and 4.7, respectively. Of special note are the results from the hydrologic simulations, Run0hyd and Run5hyd, showing greater water depths than the morphologic simulations near the mouth of the river and further upstream. This effect is due to the fixed riverbanks of the hydrologic simulation, not allowing erosion to widen or deepen the river for a higher discharge capacity in the channel. The largest difference occurs at the river mouth, where erosion of the banks and riverbed allows for a higher discharge capacity, resulting in lower water levels. Due to the V-shaped valley bathymetry, the water depth keeps increasing even when it overflows its banks at a height of 1 m. Comparing Figure 4.6 (c) and Figure 4.7 (c), this effect is amplified by the increase in precipitation. In Figure 4.6 (c) the overflowing effect is observed up to y-coordinate 4000. In Figure 4.7 (c), this continues further up the river, past y-coordinate 6000. Because of

the fixed discharge capacity of the river channel, a model without morphology may predict flooding in the wrong areas. In reality, the capacity of a river is adjusted through morphological changes. A model predicting flooding in the wrong areas can have consequences in flood planning and management. The differences in waterlevels between a morphologic and hydrologic model in this scenario are $\sim$10 cm. This is not an extreme case, however it showcases the principle of channel adjustment in response to discharge.

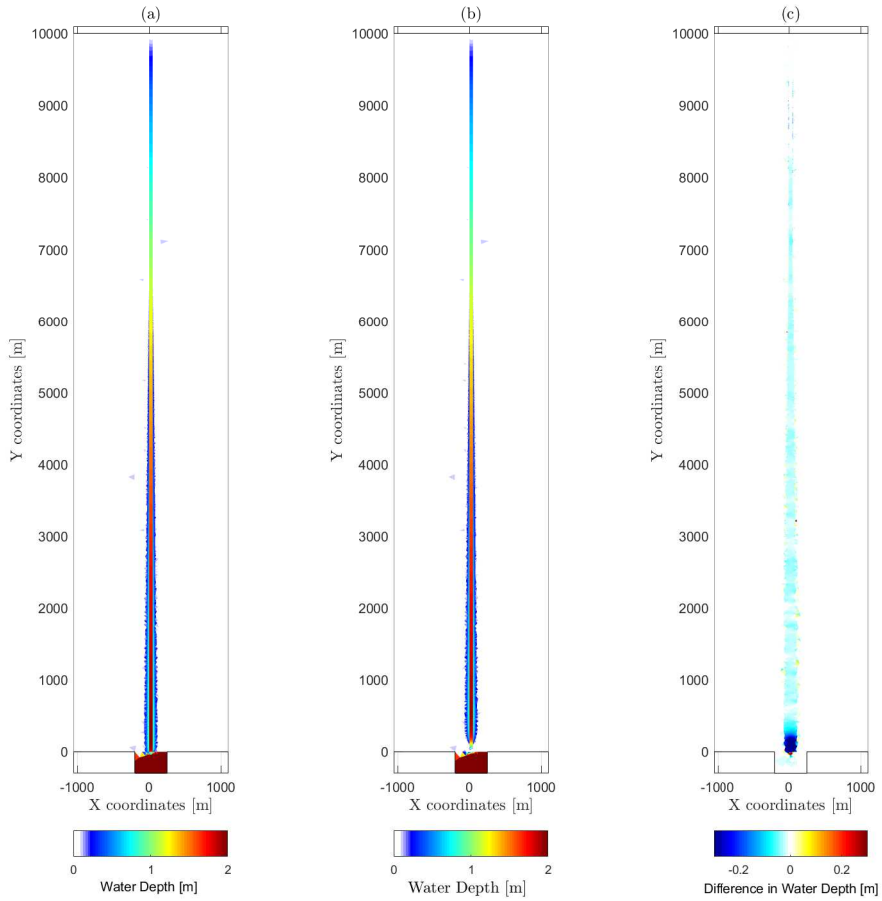

Figure 4.6: Water depth after 5 hours. The simulation with only hydrology, Run0hyd, is shown in (a), the simulation with morphology, Run0, is shown in (b). The difference between (a) and (b) is shown in (c).

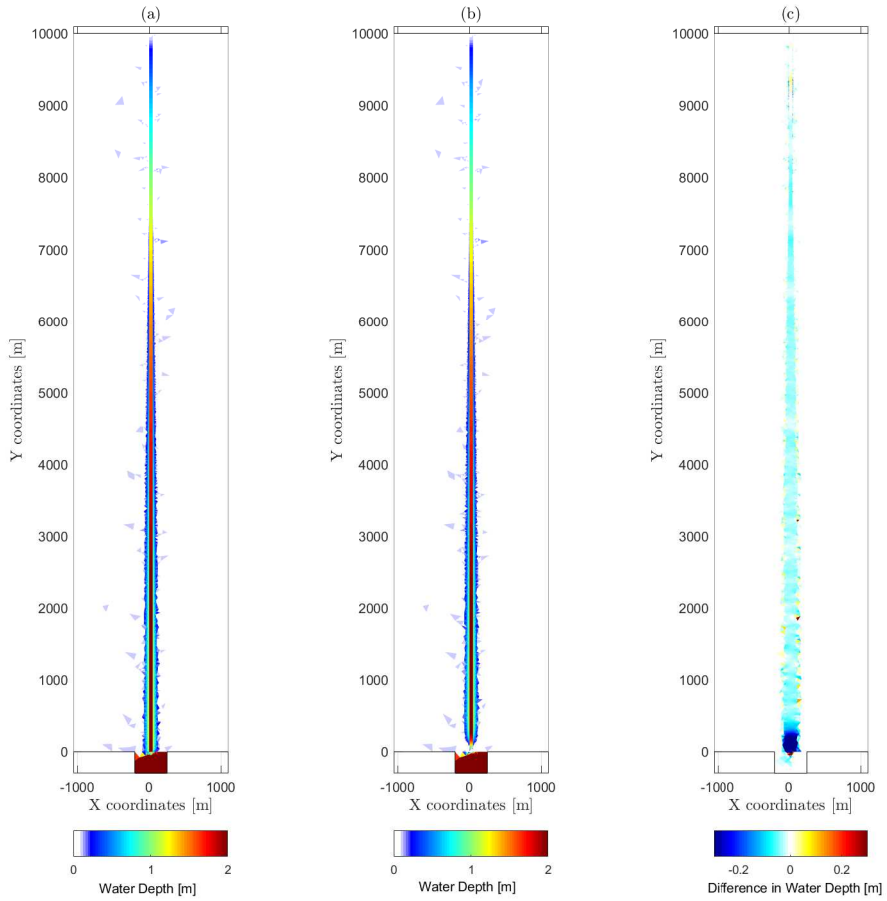

Figure 4.7: Water depth after 5 hours. The simulation with only hydrology, Run5hyd, is shown in (a), the simulation with morphology, Run5, is shown in (b). The difference between (a) and (b) is shown in (c).

4.2 Variable gradient scenario

4.2.1 Bathymetry and river-profile

The variable gradient scenario utilizes the same computational grid as the uniform gradient scenario, as well as the same model settings and boundary conditions for the simulations. The bathymetry and longitudinal river-profile are shown in Figure 4.8. To investigate the morphologic effects of variable slopes, the river has segments with different slope steepness (Figure 4.8.

Table 4.2 indicates the y-slopes applied in the different segments of the river. The surrounding terrain matches the slopes of the river in the y-direction, and has a slope in the x-direction of 1.3%. There is a 1 m difference between the river course and the surrounding terrain. The maximum height in the terrain is 55 m. A layer of 2 m is allowed to erode, to avoid mass erosion in certain cells.

Segment (km)	10-7	7-6	6-5	5-4	4-3	3-2	2-0
Slope (%)	0.28	0.83	0.28	0.56	0.28	0.42	0.28

Table 4.2: Describes the slopes of the different segments in the river, as shown in Figure 4.8. Segments refer to distance from river mouth (y-coordinates)

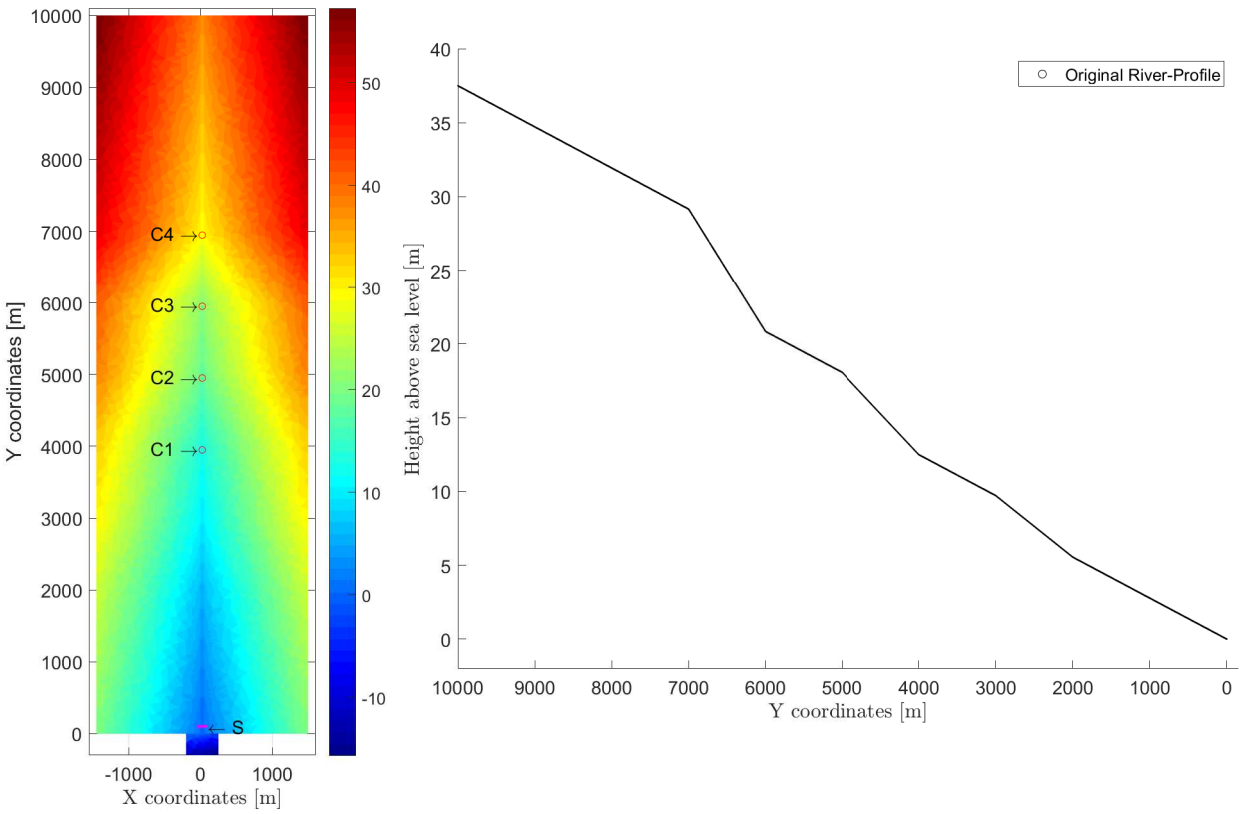

Figure 4.8: Bathymetry of the variable gradient scenario, in meters above sea level (a). The original longitudinal river-profile is shown in (b). C indicates Control Stations, S indicates the Section.

4.2.2 Results

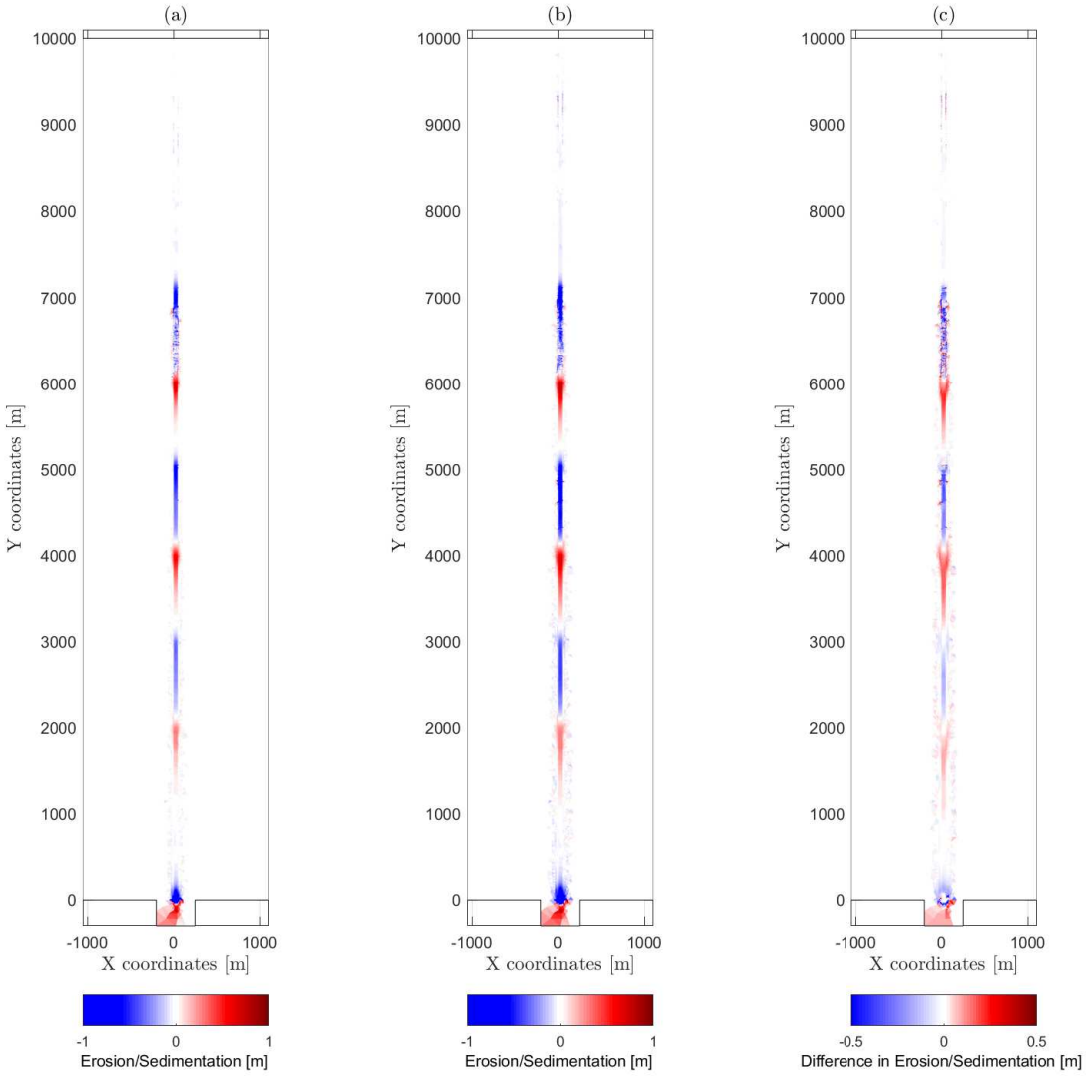

Figure 4.9: Erosion and sedimentation in the Variable Gradient Scenario, after 5 hours. The result from the baseline rainfall, Run0, is depicted in (a), and from a 50% increase in rainfall, Run5, in (b). The difference between (a) and (b) is shown in (c)

The morphologic results from Run0 and Run5 are represented in Figure 4.9.

Instead of the steady erosion of the bed, observed in the Uniform Gradient Scenario (Figure 4.2), there is erosion and sedimentation throughout the river channel. Sediment from segments of the river with a steeper slope are deposited in the gentler sections below. This flattens out the riverbed, progressing towards an equilibrium in the flow gradient. Figure 4.10 represents the longitudinal river-profile at the end of Run0 and Run5. The segments with the steepest slope, as expected, shows the greatest erosion. At y-coordinate, 6000 the sediment from the steeper river segment above is deposited. This entirely blocks the river course with sediment (Figure 4.9), to the point of depositing sediment beyond the banks of the river.

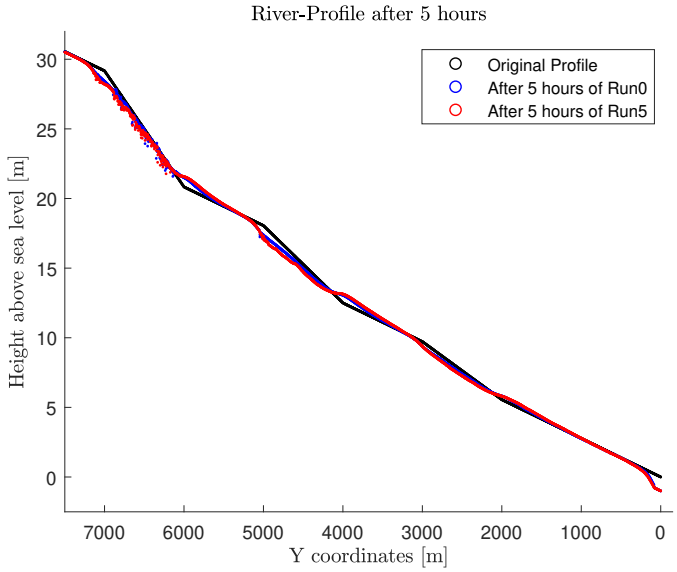

Figure 4.10: Longitudinal profiles after 5 hours of Run0, Run5 and the original profile for reference. Erosion and sedimentation flattens out the river bed.

Changes in bed level at Control Stations 1 through 4 (Figure 4.8) are represented in Figure 4.11. The bed level at Station 2, at y-coordinate 5000 (Figure 4.2), is lowered by 0.5 m due to erosion. This sediment deposits in the segment below where Station 1 is located, at y-coordinate 4000. This is caused by the fact that the upstream segment of the river is twice as steep as the downstream segment. The same effect is observed at Station 3 and Station 4. Here, the slope of the steep segment is three times that of the gentler segment. The bedlevel at Station 4, at y-coordinate 7000, is lowered by 1 m from erosion (Figure 4.9, 4.11 (b)). The sediment is deposited downstream at Station 3, at y-coordinate 6000. The results imply that a higher slope leads to more erosion in the steeper segment and sedimentation in the gentle slope segment.

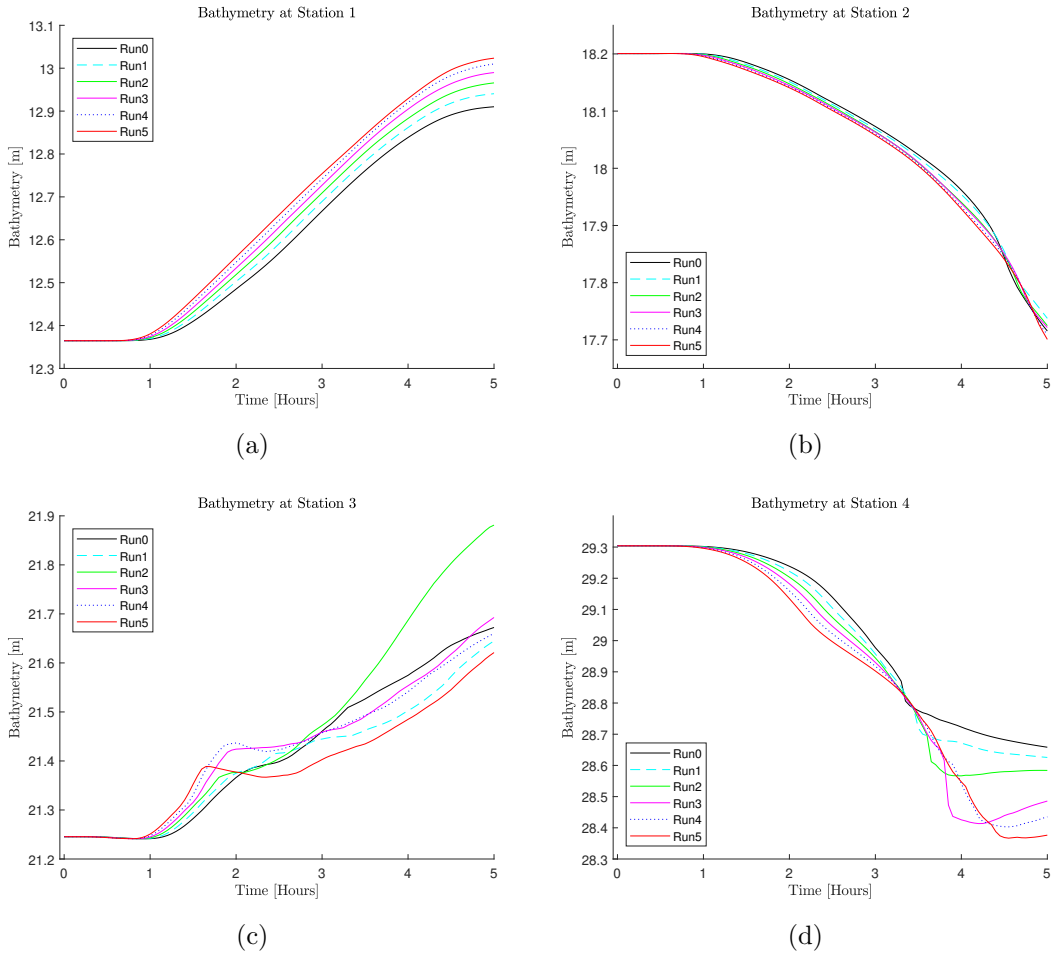

Figure 4.11: Bathymetry at Control Stations 1 through 4, over 5 hours. Shows Run0 through Run5 . The Control Stations are indicated in Figure 4.8

The sediment discharge rate and cumulative sediment discharge through Section S (Figure 4.8), located near the river mouth, are shown in Figure 4.12. Both the rate and the cumulative discharge are similar to the uniform gradient scenario, where Run5 has twice the amount sediment transported through the section as Run0.

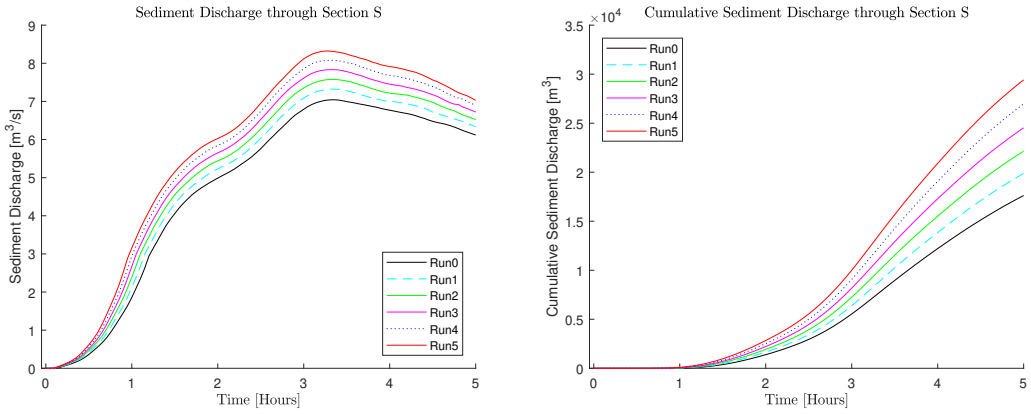

(a) (b)

Figure 4.12: Sediment discharge through section S (a), and cumulative sediment discharge through Section S is shown in (b). Section S is indicated in Figure 4.8.

The water depths after 5 hours of Run0 and Run5 are represented in Figure 4.13, and 4.14, respectively. The sedimentation in the channel causes a blockage (Figure 4.9), lowering flow velocity and diverting the flow around it. Such a blockage causes a rise in water levels, causing flooding around the blockage. This amounts to an increase of 0.5 m in water levels in the regions with the most sedimentation (Figure 4.13 (c) and 4.14 (c)). Comparing the runs with and without morphology, the overflowing occurs in different locations throughout the river. In Run0 and Run5 the worst overflowing occurs in the river segments below the locations with sedimentation, particularly

below y-coordinates 6000, 4000 and 2000. Figure 4.15 gives a closer look at the overflowing from Figure 4.13 at y-coordinate 4000. The sediment blockage in the channel rises waterlevels and causes flooding on the banks. The hydrologic runs, Run0hyd and Run5hyd, have a similar overflowing pattern to the uniform gradient scenario. A hydrologic model does not predict flooding in areas with changes in slope, caused by sedimentation and blockages in the channel. If the channel is large enough to handle the discharge, a hydrologic simulation might not show any flooding at all. Comparing Figure 4.13 (c) and 4.14 (c), an increase in rainfall intensity amplifies the differences between a hydrologic and morphologic simulation. There is a larger flooding below areas with sedimentation, and lower water levels where the channel capacity is increased due to deepening and widening caused by erosion.

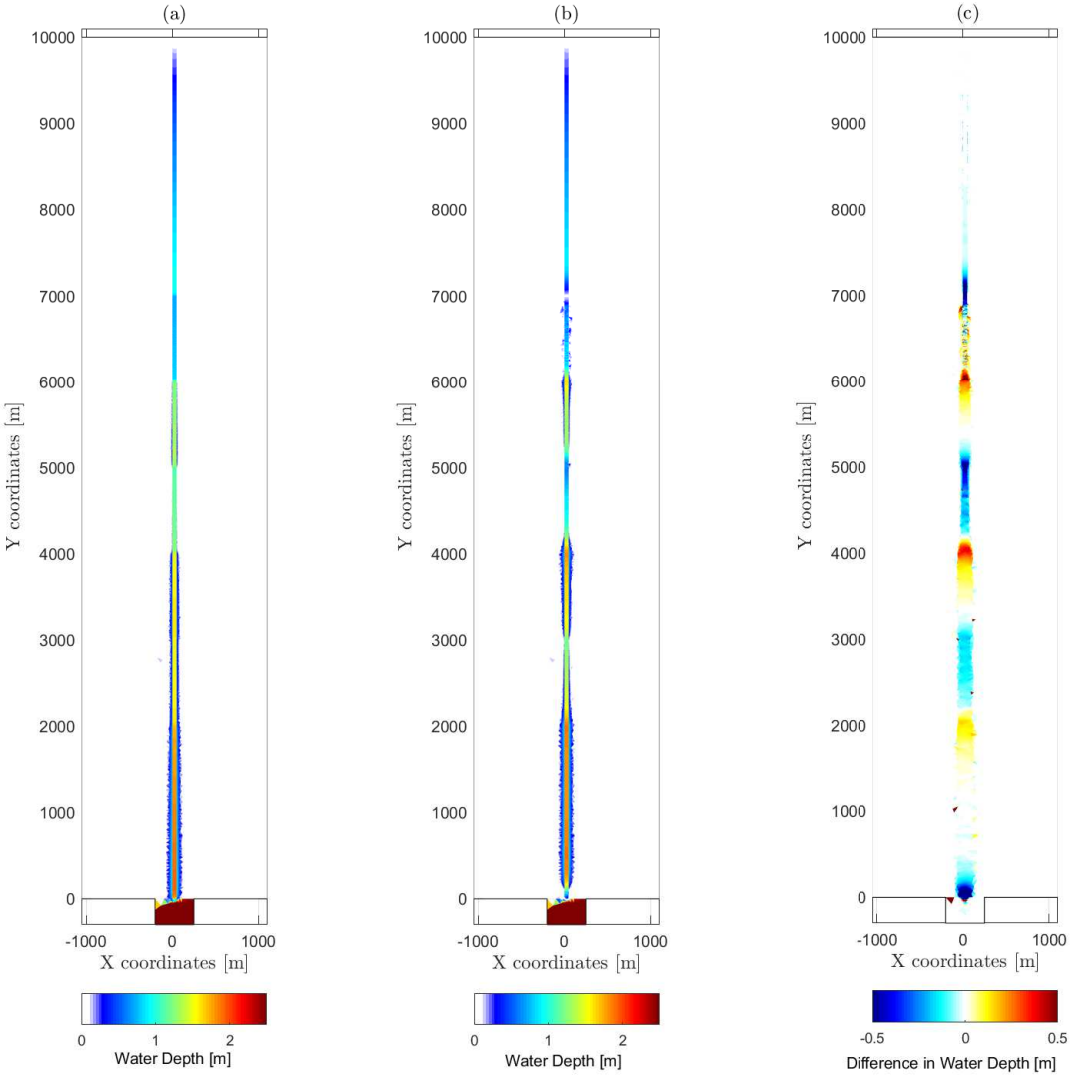

Figure 4.13: Water depth after 5 hours. The simulation with only hydrology, Run0hyd, is shown in (a), the simulation with morphology, Run0, is shown in (b). The difference between (a) and (b) is shown in (c).

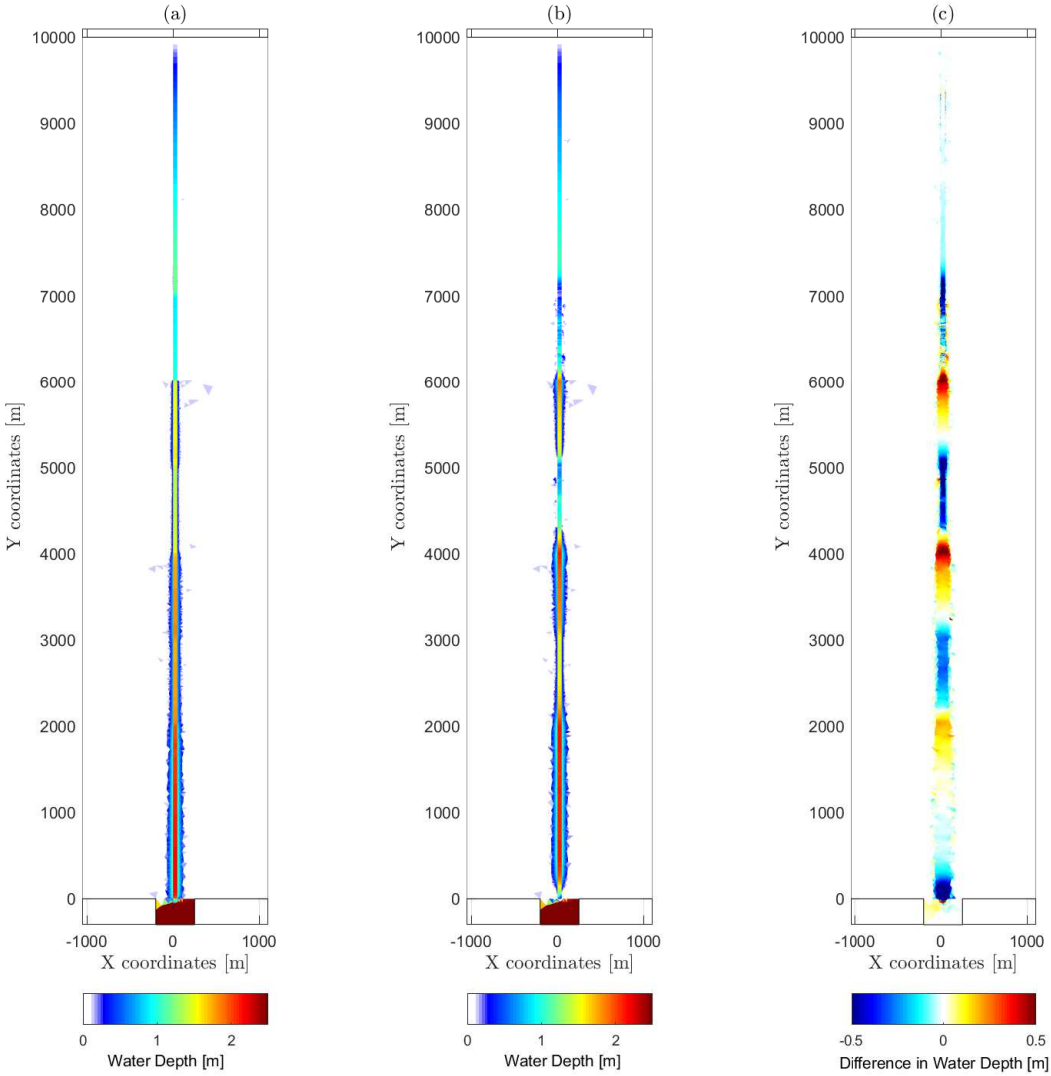

Figure 4.14: Water depth after 5 hours. The simulation with only hydrology, Run5hyd, is shown in (a), the simulation with morphology, Run5, is shown in (b). The difference between (a) and (b) is shown in (c).

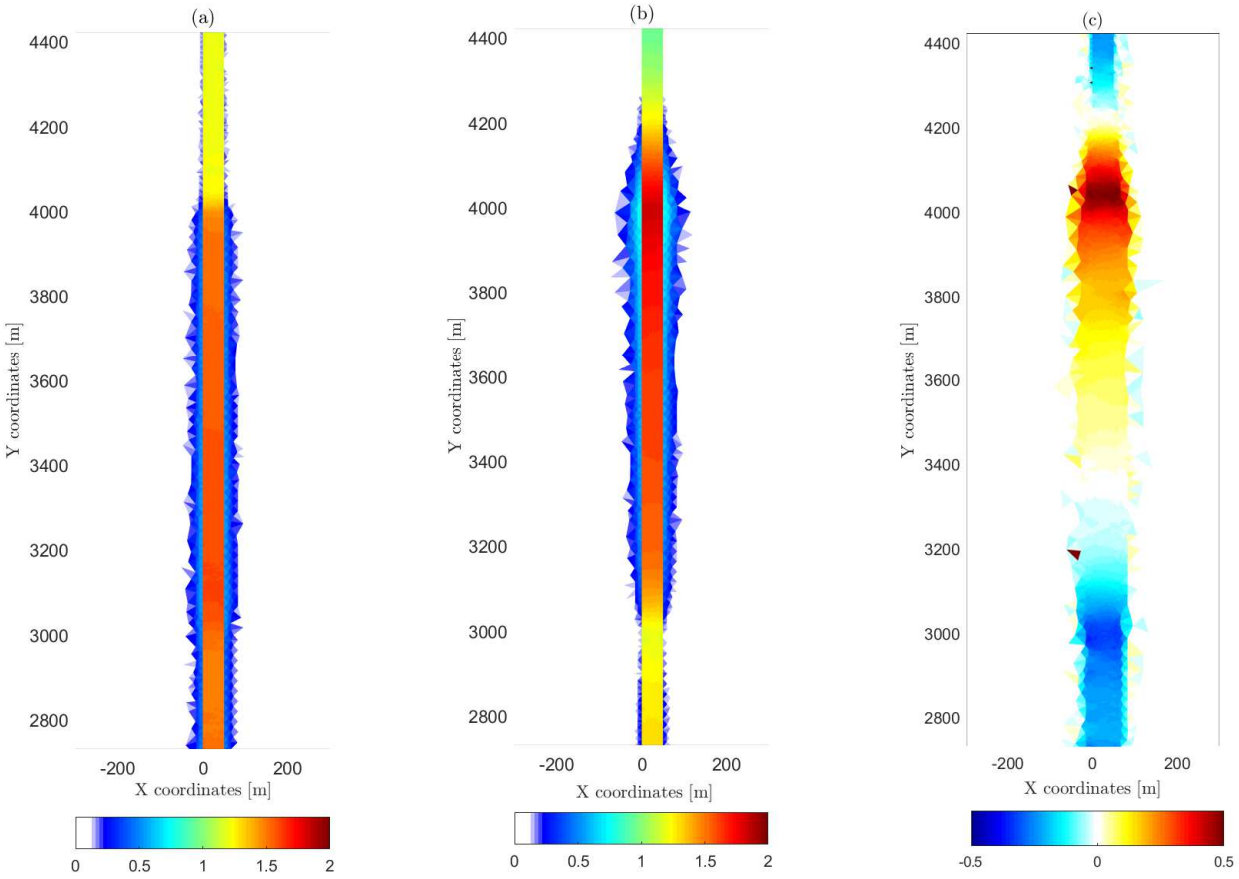

Figure 4.15: Water Depth after 5 hours. Zoomed in on the overflowing caused by the blockage in the river channel at y-coordinate 4000 in Figure 4.13. Run0hyd is shown in (a), Run0 shown in (b). The difference between (a) and (b) is shown in (c).

4.3 Steep mountain river scenario

4.3.1 Computational grid, bathymetry and model settings

In the steep mountain river scenario, there is a 18 km^2 large catchment area, where the computational grid is shown in Figure 4.16. A large part of the catchment area is located upstream, in mountainous terrain, where runoff gathers in a river course leading to the sea. There is a straight, 30 m wide, river course going through the center of the grid. The river course starts at y-coordinate 4000, and leads to the sea at y-coordinate 0, where the flow direction is downward.

Holes in the grid represents buildings of various sizes, located in the downstream flatter area. The buildings are set as non-erodible, with the assumption that they withstand the water- and sediment-masses.

Only the areas of interest have a fine resolution. The resolution of the grid is set at 100 m^2, with a finer resolution of 3 m^2 in and around the river course below y-coordinate 1200, and 10 m^2 above, with interpolation between these resolutions for a smoother grid. There is a total of 101,416 elements, with a runtime of $\sim$3 hours on a 2-core 2.30 GHz processor.

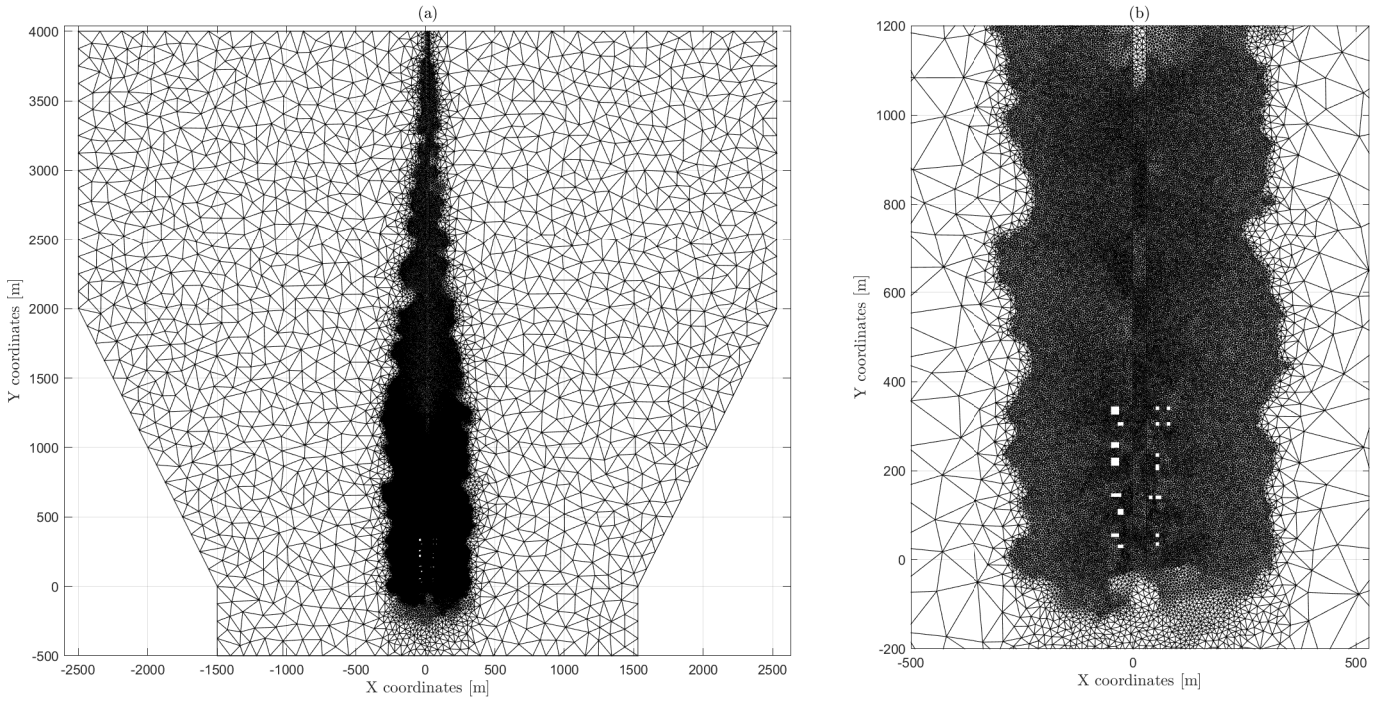

Figure 4.16: Computational grid for the steep mountain river scenario. The whole catchment area is shown in (a). The area of interest is shown in (b), where holes indicate buildings.

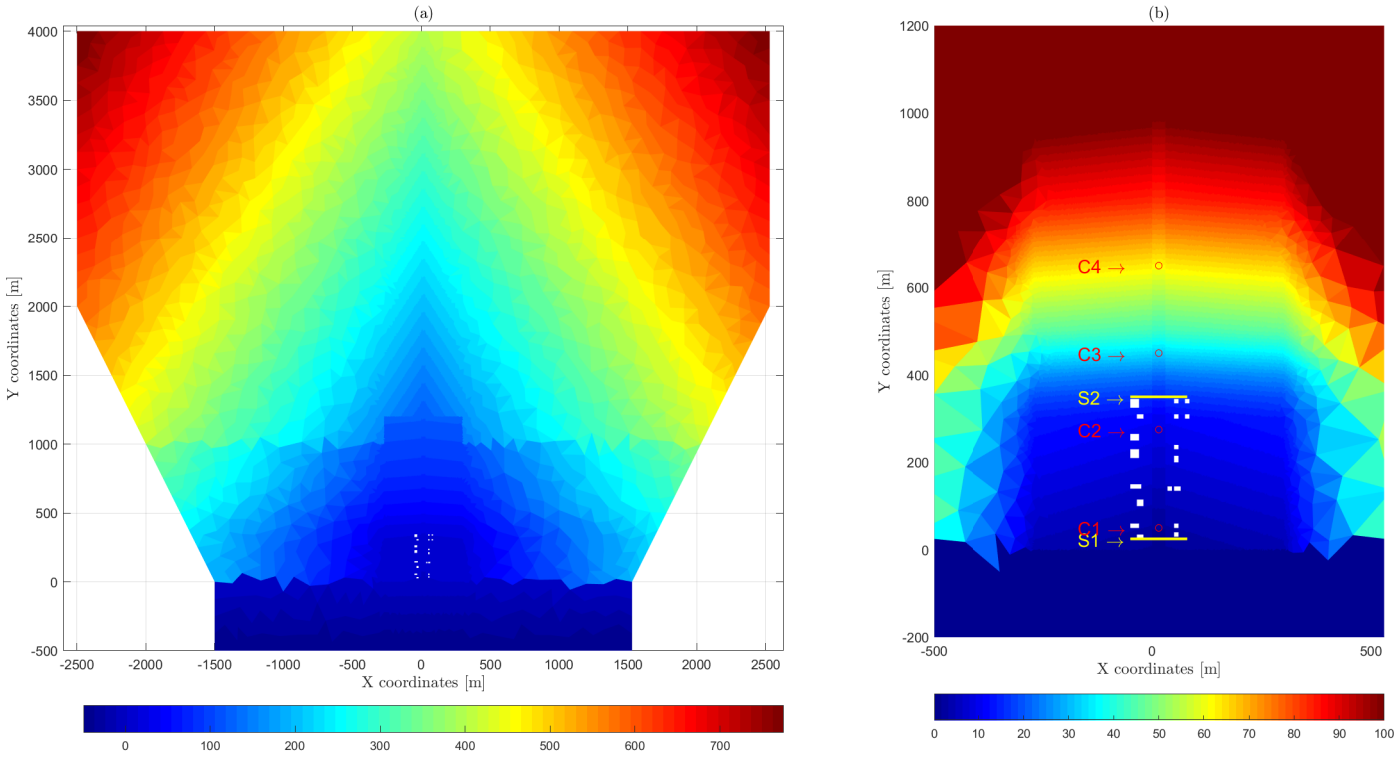

Figure 4.17: Bathymetry for the steep mountain river. The whole catchment (a), and the area of interest (b). Yellow lines indicate sections, red dots indicate control stations. White holes indicate buildings.

The bathymetry of the catchment is shown in Figure 4.17. The max height in the terrain is 775 m, which goes down to 0 m at the river outlet. In the terrain, the slope in the x-direction is 15%, so that most of the runoff is lead to the river course. Above y-coordinate 1000, the slope of the river and terrain in the y-direction is 10%. Figure 4.18 shows the longitudinal river profile below y-coordinate 1000, where segments of the river upstream

are steeper than downstream. Below y-coordinate 300 the terrain and river are gentler, making this an area typical for human activity and settlements (Midttømme, 2011). There is a height difference of 1.5 m between the river course and the surrounding terrain. Throughout the catchment, a layer of 4 m is allowed to erode. A higher roughness of 50 cm is used in this scenario, to more realistically reflect a catchment with vegetation and forests. The simulations run with the rainfall intensities shown in Table 4.1.

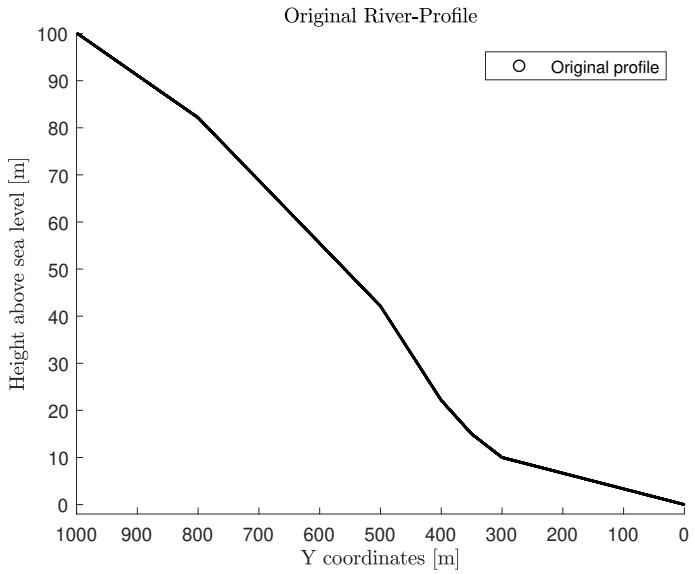

Figure 4.18: Original down-stream longitudinal river-profile in the Steep Mountain River

4.3.2 Results

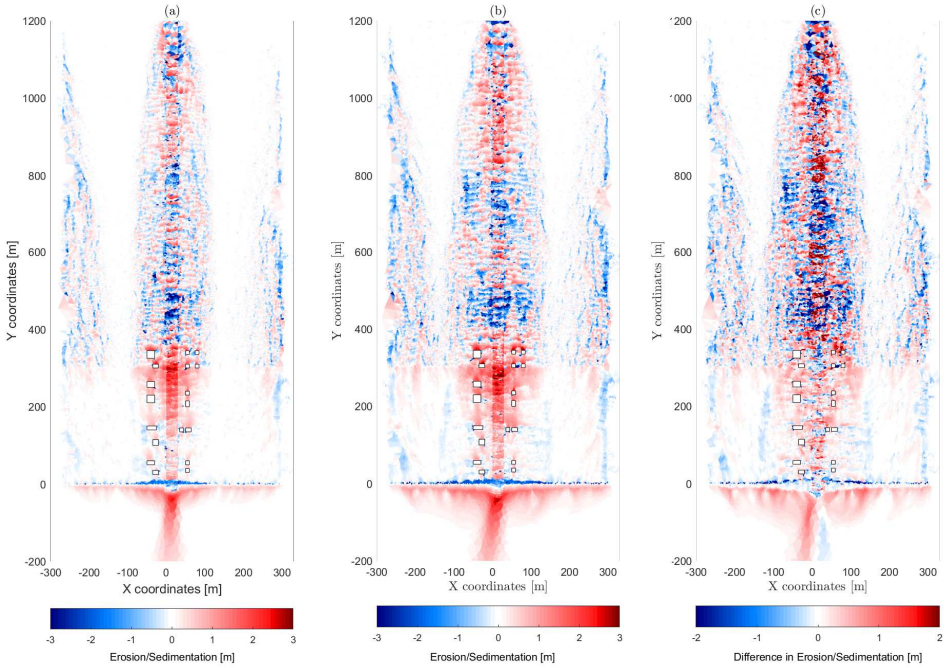

Figure 4.19: Erosion and sedimentation after 5 hours. Run0 depicted in (a), Run5 in (b). The difference between (a) and (b) is shown in (c)

The morphologic results from Run0 and Run5, after 5 hours, are shown in Figure 4.19. There is erosion from the steeper parts of the river and terrain, especially in the segment between y-coordinates 400 and 800. Much of this sediment is deposited in the flatter regions, both in the river course and beyond it, where the buildings are located. In Run5, the erosion occurs over a wider area beyond the river, and deposits a larger amount of sediment in the settlement. The erosion and sedimentation on either side of the main river, around x-coordinates -300 and 300, occurs due to the bathymetry of the catchment, creating parallel streams in the flatter parts of the catchment.

Investigation of the main river will be the focus in describing the results.

Figure 4.20 shows the absolute velocity for Run0hyd and Run0, at peak discharge. Without morphology the flood is in large part contained in the original river channel, with overflowing water following closely, parallel, to the river. The uppermost buildings still get affected by overflowing water, while the others are only slightly affected. The velocity in the river channel in Run0hyd is higher than in Run0. The sedimentation in the river pushes the water levels up and spreads the flow, causing lower flow velocity. This effect is most noticeable at y-coordinate 350, where the entire original river channel is blocked with sediment (Figure 4.19), causing new streams to divert through and around the settlement, before eventually joining the original channel near the river mouth.

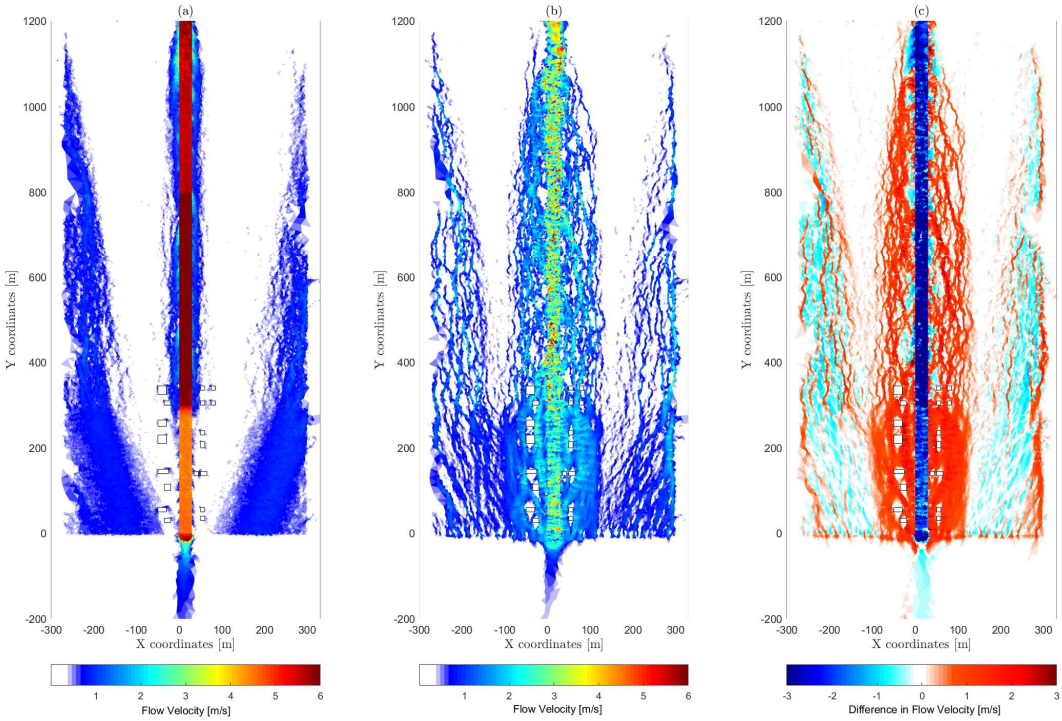

Figure 4.20: Absolute velocity after 3 hours and 30 minutes of the baseline rainfall. The simulation with hydrology only, Run0hyd, is depicted in (a), the simulation with morphology, Run0, is depicted in in (b). The difference between (a) and (b) is shown in (c)

Figure 4.21 depicts the flow velocity at peak discharge with an increase in precipitation, Run5 and Run5hyd. Again, the hydrologic simulation shows some overflowing, with high velocities in the original channel. In terms of overflowing, Run0hyd and Run5hyd have similar results, the main difference is the higher velocity in the river channel of Run5hyd (Figures 4.20, **?**). The morphologic simulations display larger difference. In Run5, the overflowing is more pronounced, and has a wider area of influence.

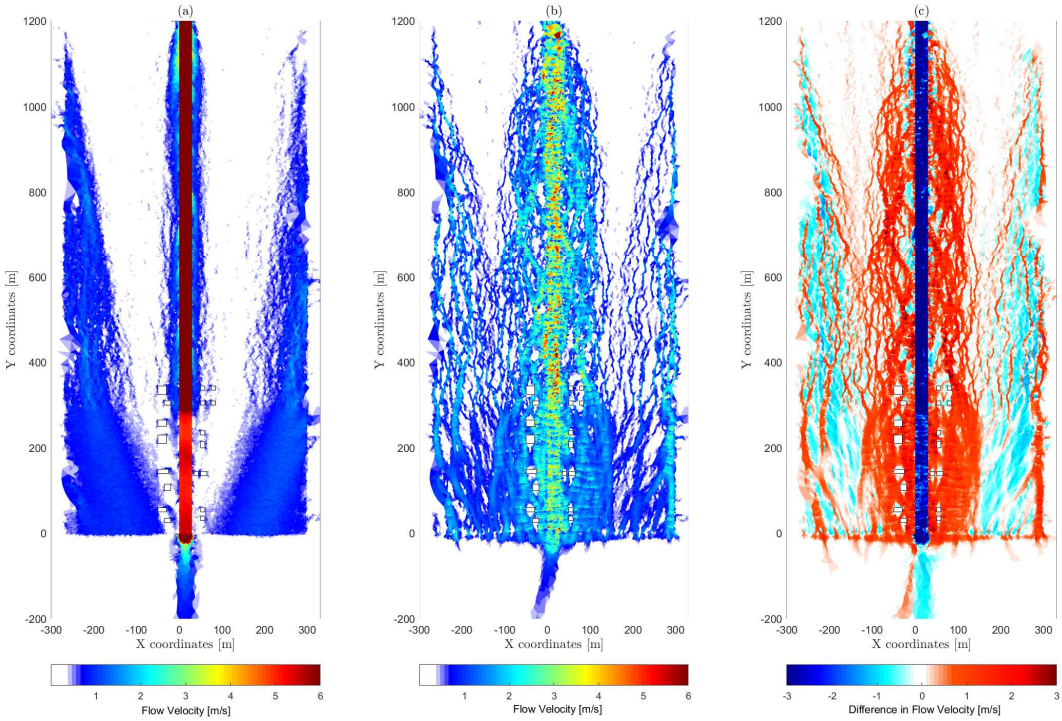

Figure 4.21: Absolute velocity after 3 hours and 30 minutes of the 50% increase in rainfall. The simulation with hydrology only, Run5hyd, is depicted in (a), the simulation with morphology, Run5, is depicted in in (b). The difference between (a) and (b) is shown in (c)

Figure 4.22 shows the bathymetry at Control Stations 1 through 4 (Figure 4.17). Due to the steeper slopes and more compact catchment, the morphologic response happens faster in this scenario than the previous two, with changes happening after 30 minutes. Observing the trends, there is considerable sedimentation and erosion occurring after 1.5 hours, even before hitting peak discharge. Changes in bed level amounts to several meters in the river course, matching observations from Figure 4.19.

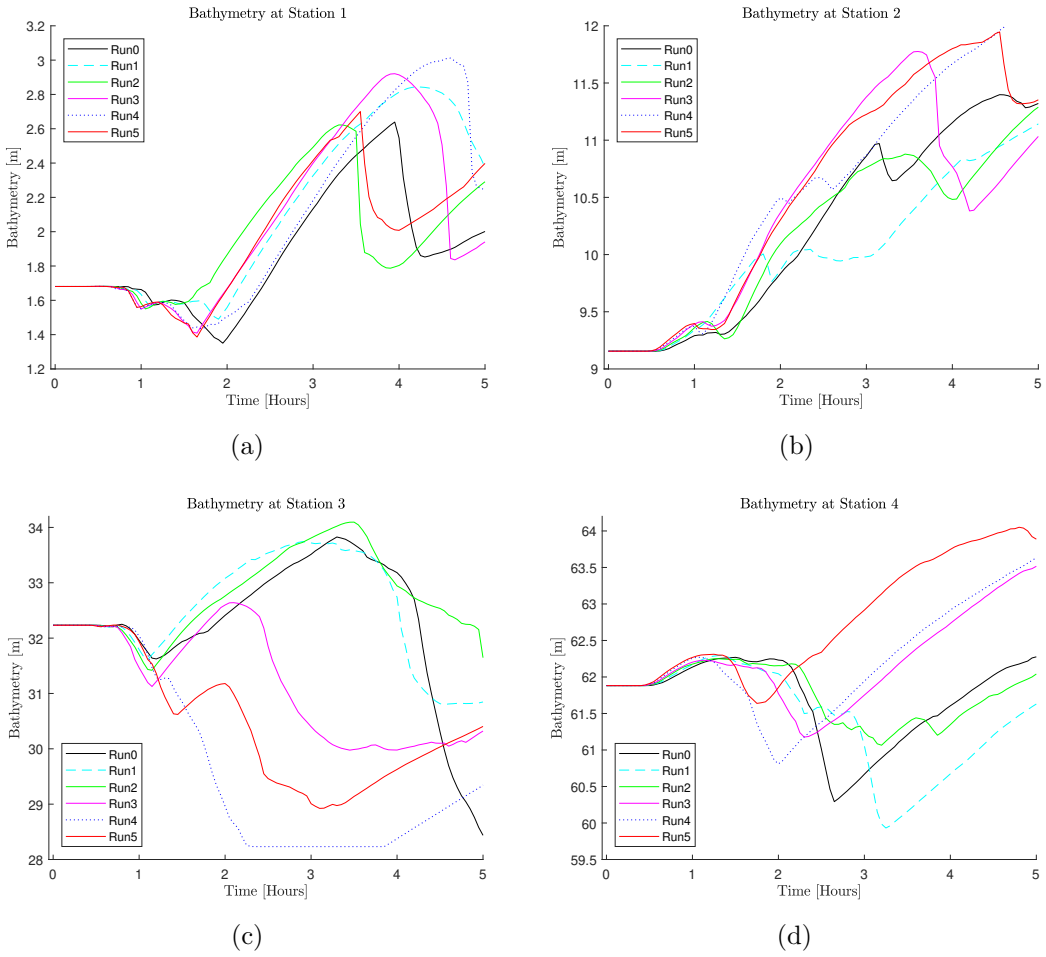

Figure 4.22: Bathymetry at Control Stations 1 through 4, over 5 hours. Shows Run0 through Run5 . The Control Stations are indicated in Figure 4.17

The sediment discharge rates and cumulative discharges for Section 1 and 2 are shown in Figure 4.23. An interesting observation is that the upstream section (Section 2), has twice as much cumulative sediment discharge as the downstream section (Section 1). This difference is due to the deposition of the sediment in the flatter area.

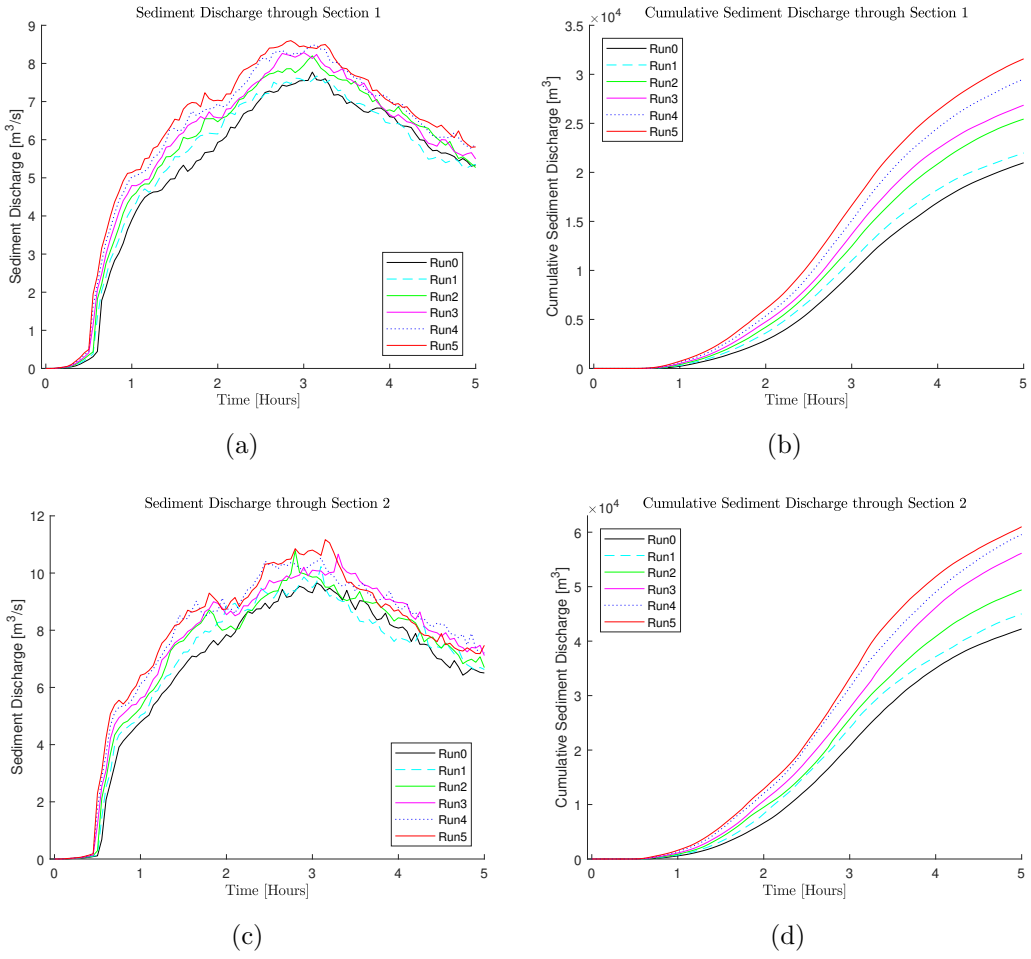

Figure 4.23: Shows discharge rate and cumulative discharge for Section 1, (a) and (b), and Section 2, (c) and (d). Section 1 and 2 are indicated in Figure 4.17 (b)

Chapter 5

Discussion

The cumulative sediment discharge results from all 3 scenarios (Figures 4.5, 4.12, 4.23) implies that a 50% increase in precipitation, doubles the amount of sediment transported. This means that the expected increase in precipitation intensity caused by climate change (Midttømme, 2011), will result not only in a higher water discharge, but also lead to more sediment transport during a flooding event. Similar findings were made by Mohamadi & Kavian (2015) and Kandel et al. (2004), where an increase in rainfall intensity had a non-linear, or exponential, response in soil erosion and sediment transport in real catchments. This implies that flood events greatly increase sediment transport in a river, making morphological changes a relevant process to consider in a flood mapping study. This exponential response is best quantified by investigating results from the Uniform Gradient Scenario and the Variable Gradient Scenario, where most of the transported sediment passes through the section near the river mouth (Figure 4.5, 4.12). Downstream areas where slopes flatten out (see Utvik and the Steep Mountain River Scenario Figure 2.1 and 4.19), are thus affected in two ways by an increase in rainfall intensity. First, the increased rainfall leads to higher discharges in the river.

Secondly, the sediment transport is increased exponentially, which leads to more sedimentation downstream, and a more widespread flooding.

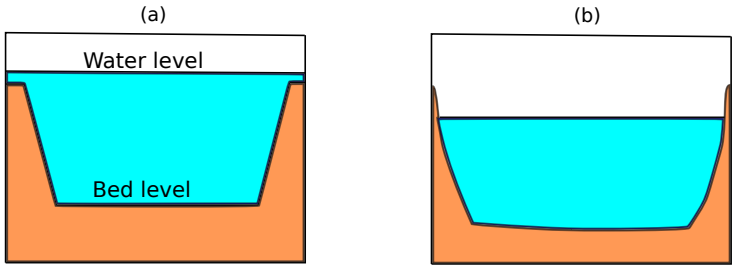

Figure 5.1: Schematic, cross-sectional representation of the widening and deepening of a river channel. In a hydrologic simulation the channel does not adjust to the discharge rate in the river, and thus overflows (a). In a morphologic simulation the channel can adjust to the discharge by deepening and/or widening of the channel, increasing the capacity lowering the water level.

For rivers with gentle gradients and small variations in slope, results from the Uniform Gradient Scenario indicates that differences between a hydrologic and morphologic simulation are relatively small for a single flood event. In the morphologic simulation, the channel capacity is increased mostly by bed erosion and widening of the river mouth (Figure 4.2), represented schematicly in Figure 5.1. This results in slightly lower water levels throughout most of the channel compared to the hydrologic simulations (Figure 4.6, 4.7). These small changes in water levels can be sensitive to uncertainties in boundary conditions and model settings, in line with the findings of Wong et al. (2014). Due to the uniform gradient, all the sediment is transported to the

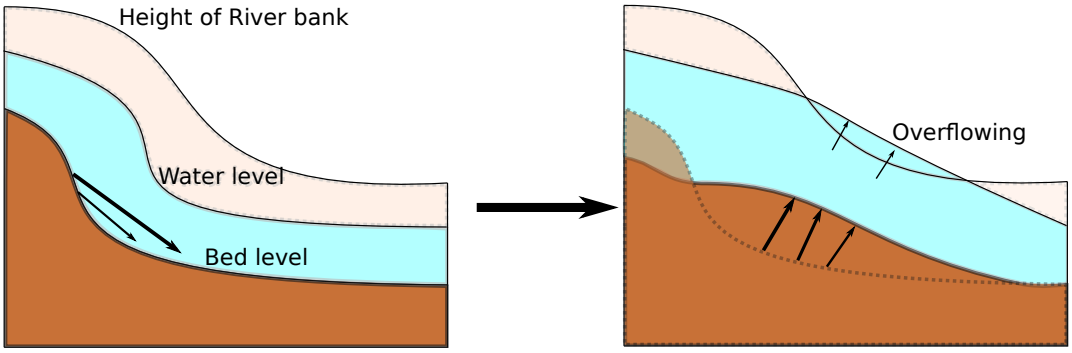

Figure 5.2: Schematic representation of the overflowing caused by the morphologic response to variations in slopes. Sediment from the steep segment above, where velocity is large, is desposited in the segment with a gentler slope below, where velocity decreases. Notice also the flattening of the river bed. This pushes the water level up, to the point of overflowing the river banks.

sea, not causing blockages in the river channel. In rivers with uniform flow conditions, such as flow direction, slopes and velocity, a flood map created with a hydrologic simulation might be sufficient. However, real rivers do not have uniform flow conditions. Meandering, varying widths of the river channel, and differences in sediment build-up and sizes, all cause variations in flow-regime in a river channel. In the Uniform Gradient Scenario, the only changes in flow conditions takes place at the river mouth, where the most notable morphologic response occurs. Buildings located near the riverbank would be destroyed, such as in the flood in Flåm (Figure 2.3). Incorporating river segments with varying widths or depths, meandering etc., in the simulation, should show results more closely resembling the erosion that took place in Flåm.

In the Variable Gradient Scenario, the morphologic effects of different flow conditions caused by variations in slope, are more closely investigated (Figure 4.9). The steeper slopes cause increased velocity, and therefore more erosion of sediment, which deposits when the river slope become gentler, and velocity decreases (Figure 5.2). The larger the difference in slope between two river segments, the more sediment is transported downstream to the gentle segment. The longitudinal profile (Figure 4.10) demonstrates how the river-profile tends to flatten out to reach an equilibrium. The sediment deposited in the flatter river segments create blockages in the river course, and lead to an increase in water levels of up to 0.5 m. In a flooding event, this difference can result in a large increase in damages. In terrain with flatter floodplains, these sediment-blockages may divert and spread sediment and water masses across settlements and infrastructure. This effect makes human activity located in the flatter regions downstream from a steep catchment especially vulnerable to overland flow diverted by sediment blockages in the river channel (Figure 5.2). Many municipalities in western Norway are located in catchments with these characteristics (Midttømme, 2011), which makes it questionable whether a hydrologic model is adequate for use in flood maps in these regions, with a large difference in slope.

The Steep Mountain River Scenario demonstrates the difference between a hydrologic and a morphologic simulation, in a catchment with steep upstream terrain, and a flatter downstream segment. The hydrologic simulation fails to show the formation of new water courses through and around the settlement, as a result of the, up to, 3 m high blockage in the river channel (Figure 4.19). In addition to diverting the flow through the settlement (Figure 4.20, 4.21),

large amounts of sediment are also deposited, similar to the flood in Utvik (Figure 2.1). The buildings in the simulations are considered non-erodible. However, the masses of water and sediment would certainly destroy and carry the buildings with them, as was the case in Tretten (Figure 2.4). Simulations of the flood in Utvik by Dam (2017), using the same model, show similar results. A hydrologic simulation proved unable to reproduce the new stream paths formed during the flood, while a morphologic simulation showed better accuracy.

Accurate predictions in a realistic setting, however, are still questionable (Haff, 1996). Small errors in a non-linear model may lead to unexpected results. In addition to higher computational cost than a hydrologic simulation, there are several challenges in data collection and model settings tied to a morphologic model (Haff, 1996).

Empirical sediment transport formulae are derived in laboratories, thus the translation to a geomorphic scale is debatable. The formula used in this study is mostly meant for fine sediment sizes and does not have a critical shear stress component (Engelund F., 1967). This makes it unsuited for larger grain sizes than used in this study (1 cm), and outcomes may drastically change for larger sediment classes. Further simulations with different formulae should be considered for comparison with the results.

Collecting precise sediment and roughness data for a flood map requires considerable effort. The single grain size used in this study is a simplification of reality, where a catchment has large differences in sediment classes throughout. The scenarios run in this thesis are quantitively sensitive with

regards to finer grain sizes, but qualitatively stable within a reasonable range ($\sim$0.5 cm). This means that erosion and sedimentation occur in the same locations, where the grain size influences the magnitude. Smaller grain sizes increase the sediment transport, while larger sizes decrease it. For larger grain sizes, the results become unreliable with the formula used, and a different sediment transport formula should be considered.

Roughness is an important input parameter, because of the effect it has on shear stresses and velocities, and in turn, on sediment transport. Roughness data is hard to determine, since it is highly variable throughout the terrain. A global roughness is therefore a simplification, and a potential source for uncertainty. Even with the relatively simple terrains and river channels used in the scenarios, changes in roughness has a considerable impact on qualitative morphological outcomes. As with grain size, changes in roughness in the scenarios only changes the magnitude of morphologic change, however the changes occur in the same locations. An increase in roughness (+10 cm) has a negative effect on sediment transport in the Uniform Gradient and Variable Gradient scenarios. This is due to the gentle slopes, where an increase in roughness has a considerable effect on the flow velocity. The Steep Mountain River Scenario is not very sensitive to a change in roughness ($\pm$10 cm). In this case, the geophysical factors (e.g. steep slopes and terrain layout) are more important than the input parameters. Thus, in a morphologic simulation, uncertainties in parameter inputs may be overruled by the morphologic behavior of the model, driven by the geophysical characteristics of the catchment.

The reliability of morphologic modelling is still under debate (Wong et al.,

2014; Neuhold et al., 2009; Guan et al., 2015, 2016; Lane et al., 2007; Merwade et al., 2008), due to the increased complexity and strong non-linear behavior, as compared to a strictly hydrological model. However, there are numerous studies showcasing the ability of morphodynamic models to accurately hindcast morphologic changes (Guan et al., 2015, 2016; Gharbi et al., 2016). Good accuracy on the scale of centuries can also be obtained in hindcasts, e.g. Dam et al. (2016). The same model as used in this thesis was applied on an estuary over a 110-year period, with successful results. It is believed that a morphologic model can overcome its associated uncertainties because of the physical nature of rivers to find a flow equilibrium (Dam et al., 2016; Dam, 2017; Blom et al., 2017). This is supported by the results in this thesis, where changing parameters only has a quantitative effect. Morphologic changes are largely dependent on slope and changes in flow regimes due to geophysical factors (Figures 4.2, 4.9, 4.19). The behavior of morphologic models to reach these equilibriums may thus make morphologic changes in a flood event predictable, overruling the uncertainties associated with them. Advantages of using a morphologic model also include predicting new flood paths caused by morphologic changes, which a hydrologic model is unable to (Dam, 2017). Considering these factors, the use of morphologic models in flood maps may have significant benefits over hydrological models. With the future increase in rainfall intensity caused by climate change, the advantages of using morphologic models in flood maps may become more relevant.

Chapter 6

Conclusions

In this thesis, the morphologic changes during a pluvial flood, and the impact of an increase in rainfall intensity caused by climate change, have been investigated. The 2-D morphologic model FINEL2D was applied to 3 scenarios with different characteristics, over a 5 hour rainfall course.

With a 50% increase in rainfall, the results reflected a doubling in the amount of sediment transported during the flood events. This implies an exponential relationship between rainfall and sediment transport. In the scenarios with non-uniform river bed slopes, sediment is eroded from river segments with steep slopes, and deposited in segments with gentler slopes. In the Variable Gradient Scenario, this results in a flattening of the bed, where the model attempts to reach a flow equilibrium, in line with findings from (Dam et al., 2016), (Dam, 2017) and (Blom et al., 2017).

The Steep Mountain Scenario showcases a large difference in results of a hydrological model, versus a morphological one. Sediment depositing and blocking a river channel causes the flow to be pushed up (Figure 5.2), divert-

ing to areas with potential human activity.

The use of morphologic models in flood maps have been discussed. Morphologic models have been shown to accurately hindcast previous flood events and long-term morphologic changes. The incorporation of a strongly non-linear morphodynamic module introduces new sources of uncertainty, as compared to a hydrological model. The uncertainties introduced are argued to be overruled by the morphologic behavior of the model caused by the catchment characteristics, making morphological changes in large part predictable. In conjunction with other benefits of incorporating morphological changes, such as predicting new flood paths caused by morphologic changes, it is concluded that there are potential advantages of using a morphological model in flood maps.

With an increase in rainfall caused by climate change, and the exponential response in sediment transport, the role of morphologic models in flood maps may become more relevant in the near future.

References

Allen, P. A. (1997, Apr). Earth surface processes. doi: 10.1002/9781444313574

Beven, K. (2001). How far can we go in distributed hydrological modelling? *Hydrology and Earth System Sciences*, *5*(1), 1–12. doi: 10.5194/hess-5-1-2001

Blom, A., Arkesteijn, L., Chavarrías, V., & Viparelli, E. (2017). The equilibrium alluvial river under variable flow and its channel-forming discharge. *Journal of Geophysical Research: Earth Surface*, *122*(10), 1924–1948. doi: 10.1002/2017jf004213

Brázdil, R., Kundzewicz, Z. W., & Benito, G. (2006). Historical hydrology for studying flood risk in europe. *Hydrological Sciences Journal*, *51*(5), 739–764. doi: 10.1623/hysj.51.5.739

Dam, G. (2017). Simulating the flooding in utvik on 24 july 2017 using a high resolution 2d hydro- and morphological model. *Unpublished Report*.

Dam, G., Bruens, A., & Bliek, A. (2006, Feb). Band width analysis morphological predictions haringvliet estuary. *River, Coastal and Estuarine Morphodynamics*. doi: 10.1201/9781439833896.ch21

Dam, G., Wegen, M. V. D., Labeur, R. J., & Roelvink, D. (2016). Modeling centuries of estuarine morphodynamics in the western scheldt estuary. *Geophysical Research Letters*, *43*(8), 3839–3847. doi: 10.1002/2015gl066725

Dewals, B., Rulot, F., Erpicum, S., Archambeau, P., & Pirotto, M. (2011). Advanced topics in sediment transport modelling: Non-alluvial beds and hyperconcentrated flows. *Sediment Transport*. doi: 10.5772/15025

Easterbrook, D. (1996). *Surface processes and landforms*. Prentice Hall; 2 edition.

Eeg J., N. (1995). *Ekstremflom vesleofsen.* Retrieved from `https://www.nrk.no/innlandet/25-ar-etter-ekstremflommen-_vesleofsen_-er-det-igjen-fare-for-en-ny-storflom-1.15013936` (Retrieved on 18.05.20)

Engelund F., H. E. (1967). *Monograph on sediment transport in alluvial streams*. Teknisk Forlag.

Evans, L. (2010, Feb). Partial differential equations. *Graduate Studies in Mathematics*. doi: 10.1090/gsm/019

Galappatti, G., & Vreugdenhil, C. B. (1985). A depth-integrated model for suspended sediment transport. *Journal of Hydraulic Research*, *23*(4), 359–377. doi: 10.1080/00221688509499345

Gharbi, M., Soualmia, A., Dartus, D., & Masbernat, L. (2016, Jan). Floods effects on rivers morphological changes application to the medjerda river in tunisia. *Journal of Hydrology and Hydromechanics*, *64*(1), 56–66. doi: 10.1515/johh-2016-0004

Guan, M., Carrivick, J. L., Wright, N. G., Sleigh, P. A., & Staines, K. E. (2016). Quantifying the combined effects of multiple extreme floods on river channel geometry and on flood hazards. *Journal of Hydrology*, *538*, 256–268. doi: 10.1016/j.jhydrol.2016.04.004

Guan, M., Wright, N., & Sleigh, A. (2015, June). Effects of river morphological change on innundation modelling during extreme flood sequences. *36th IAHR World Congress*.

Haff. (1996). Limitations on predictive modelling in geomorphology. *The Scientific Nature of Geomorphology*, 337-358.

Hansen-Bauer. (2015). Klima i norge 2100. , *Report 2/2015*. Retrieved from `https://klimaservicesenter.no/faces/mobile/article.xhtml?uri=klimaservicesenteret/klima-i-norge-2100` (Retrieved 18.05.20)

Kandel, D. D., Western, A. W., Grayson, R. B., & Turral, H. N. (2004). Process parameterization and temporal scaling in surface runoff and erosion modelling. *Hydrological Processes*, *18*(8), 1423–1446. doi: 10.1002/hyp.1421

Kundu P., D. D., Cohen I. (2016). *Fluid mechanics*. Academic Press.

Lane, S. N., Tayefi, V., Reid, S. C., Yu, D., & Hardy, R. J. (2007). Interactions between sediment delivery, channel change, climate change and flood risk in a temperate upland environment. *Earth Surface Processes and Landforms*, *32*(3), 429–446. doi: 10.1002/esp.1404

Lawrence. (2016). Klimaendringer og framtidige flommer i norge. *Norges vassdrags- og energidirektorat*, *81*.

Merwade, V., Olivera, F., Arabi, M., & Edleman, S. (2008). Uncertainty in flood inundation mapping: Current issues and future directions. *Journal of Hydrologic Engineering*, *13*(7), 608–620. doi: 10.1061/(asce)1084-0699(2008)13:7(608)

Midttømme. (2011). Retningslinjer for flomberegninger. *Norges vassdrags- og energidirektorat*.

Mikalsen, V. (2014). *Flom i flåm.* Retrieved from `https://www.vg.no/nyheter/innenriks/i/RLKKW/flommen-i-flaam-aapnet-huset-for-11-evakuerte` (Retrieved on 18.05.20)

Mohamadi, M. A., & Kavian, A. (2015). Effects of rainfall patterns on runoff and soil erosion in field plots. *International Soil and Water Conservation Research*, *3*(4), 273–281. doi: 10.1016/j.iswcr.2015.10.001

Nakayama, Y. (2018). History of fluid mechanics. *Introduction to Fluid Mechanics*, 1–7. doi: 10.1016/b978-0-08-102437-9.00001-2

Naturskader. (2019). Retrieved from `finansnorge.no/statistikk/skadeforsikring/nokkeltall/naturskade/` (Retrieved 18.05.20)

Neuhold, C., Stanzel, P., & Nachtnebel, H. P. (2009). Incorporating river morphological changes to flood risk assessment: uncertainties, methodology and application. *Natural Hazards and Earth System Sciences*, *9*(3), 789–799. doi: 10.5194/nhess-9-789-2009

Nie. (2012). Flomfrekvensanalyse og flomvannlinjeberegninger for byvassdrag. *Vann*.

Plate, E. J. (2002). Flood risk and flood management. *Journal of Hydrology*, *267*(1-2), 2–11. doi: 10.1016/s0022-1694(02)00135-x

Rawlins, C. L. (1995). A view of the river by luna b. leopold. *Western American Literature*, *29*(4), 386–386. doi: 10.1353/wal.1995.0126

Sinha, S. K., & Parker, G. (1996). Causes of concavity in longitudinal profiles of rivers. *Water Resources Research*, *32*(5), 1417–1428. doi: 10.1029/95wr03819

Slater, L. J., Singer, M. B., & Kirchner, J. W. (2015). Hydrologic versus geomorphic drivers of trends in flood hazard. *Geophysical Research Letters*, *42*(2), 370–376. doi: 10.1002/2014gl062482

Toro, E. F. (1999). Riemann solvers and numerical methods for fluid dynamics.
doi: 10.1007/978-3-662-03915-1

Tsakiris, G. (2014). Flood risk assessment: concepts, modelling, applications. *Natural Hazards and Earth System Sciences*, *14*(5), 1361–1369. doi: 10.5194/nhess-14-1361-2014

Uzunca, M. (2016). Discontinuous galerkin methods. *Adaptive Discontinuous Galerkin Methods for Non-linear Reactive Flows*, 9–25. doi: 10.1007/978-3-319-30130-3_2

van Rijn, L. C. (1993). *Principles of sediment transport in rivers, estuaries and coastal seas*. Aqua Publications.

Vågenes H., V. (2017). *Flom i utvik*. Retrieved from `vg.no/nyheter/innenriks/i/zqyjq/frakter-reserve-bro-til-utvik-haaper-veien-kan-aapnes-igjen-torsdag` (Retrieved on 18.05.20)

Vreugdenhil, C. B. (1994). Three-dimensional shallow-water flow. *Water Sci-*

ence and Technology Library Numerical Methods for Shallow-Water Flow, 217–246. doi: 10.1007/978-94-015-8354-1_11

Wong, J. S., Freer, J. E., Bates, P. D., Sear, D. A., & Stephens, E. M. (2014). Sensitivity of a hydraulic model to channel erosion uncertainty during extreme flooding. *Hydrological Processes*, *29*(2), 261–279. doi: 10.1002/hyp.10148